Quantifying demand flexibility of power-to-heat and thermal energy storage in the control of building heating systems

Finck, Christian; Li, Rongling; Kramer, Rick; Zeiler, Wim

Published in:
Applied Energy

Link to article, DOI:
10.1016/j.apenergy.2017.11.036

Publication date:
2018

Document Version
Publisher's PDF, also known as Version of record

Applied Energy 209 (2018) 409–425

Contents lists available at ScienceDirect

Applied Energy

journal homepage: www.elsevier.com/locate/apenergy

Quantifying demand flexibility of power-to-heat and thermal energy storage in the control of building heating systems

Christian Finck[a,*], Rongling Li[b], Rick Kramer[a], Wim Zeiler[a]

[a] Department of the Built Environment, Eindhoven University of Technology, de Rondom 70 5612 AP, The Netherlands
[b] Department of Civil Engineering, Technical University of Denmark, Nils Koppels Allé Building 402, 2800 Kgs. Lyngby, Denmark

HIGHLIGHTS

- Water, phase change material, and thermochemical material tanks are integrated for optimal control.
- Demand flexibility of thermal energy storage tanks integrated with a building heating system is quantified.
- Flexibility indicators representing demand flexibility are calculated for reference and optimal control.
- A power flexibility indicator is introduced, the instantaneous power flexibility.

ARTICLE INFO

Keywords:
Thermal energy storage
Demand flexibility
Optimal control
Phase change material
Thermochemical material

ABSTRACT

In the future due to continued integration of renewable energy sources, demand-side flexibility would be required for managing power grids. Building energy systems will serve as one possible source of energy flexibility. The degree of flexibility provided by building energy systems is highly restricted by power-to-heat conversion such as heat pumps and thermal energy storage possibilities of a building. To quantify building demand flexibility, it is essential to capture the dynamic response of the building energy system with thermal energy storage. To identify the maximum flexibility a building's energy system can provide, optimal control is required. In this paper, optimal control serves to determine in detail demand flexibility of an office building equipped with heat pump, electric heater, and thermal energy storage tanks. The demand flexibility is quantified using different performance indicators that sufficiently characterize flexibility in terms of size (energy), time (power) and costs. To fully describe power flexibility, the paper introduces the instantaneous power flexibility as power flexibility indicator. The instantaneous power flexibility shows the potential power flexibility of TES and power-to-heat in any case of charging, discharging or idle mode. A simulation case study is performed showing that a water tank, a phase change material tank, and a thermochemical material tank integrated with building heating system can be designed to provide flexibility with optimal control.

1. Introduction

With the increasing application of distributed energy generation, attuning energy consumption to energy generation has become an attractive mitigation strategy for intermittency issues [1]. The ability to control electrical energy consumption based on power grid incentives is called demand response (DR) [2]. Special attention has been given to the energy consumption of buildings which plays a major role in global energy demand [3]. The DR of buildings is comprised of the ability to control the electricity demand profile [3]. The deviation from the reference demand profile is the demand flexibility of buildings [3,4].

A summary of quantification methods for the energy flexibility of buildings is provided by Lopes et al. [3], in which characterization of energy flexibility refers to a demand increase as negative flexibility and a demand decrease as positive flexibility [5,6]. Nuytten et al. [7] calculated the energy flexibility of a combined heat and power (CHP) system with thermal energy storage (TES) wherein flexibility was related to shifting of the electrical consumption in time, expressed as the number of hours of delayed operation. The authors in [7] introduced the concept of forced and delayed flexibility. With forced flexibility, a period is determined in which a system is forced to store excess energy. Delayed flexibility describes a period in which a system is requested to postpone and reduce energy consumption, for instance, by discharging storage. The method of forced and delayed flexibility provides

* Corresponding author.
E-mail address: c.j.finck@tue.nl (C. Finck).

https://doi.org/10.1016/j.apenergy.2017.11.036
Received 22 July 2017; Received in revised form 2 November 2017; Accepted 4 November 2017
Available online 09 November 2017

Nomenclature

C	available storage capacity
D	effective diffusion
h	specific enthalpy
J	optimal cost function
J_π	expected costs referring to policy π
k_m	mass transfer coefficient between evaporator/condenser and adsorber
l	duration
m	number of OC events
m_{ads}	mass adsorbate
n	number
N	planning horizon
p	pressure
q	adsorbate – amount of refrigerant (water) in the solid phase of dry material (zeolite13X)
Q_s	adsorption enthalpy
t	time
u	positive constant velocity
u_t	control variables referring to optimal control
U_t	control constraints
V_{dot}	volume flow
x	spatial coordinate referring to the one-dimensional convection-diffusion equation
x_t	state variables referring to optimal control
T	temperature

Greek symbols

α	positive constant coefficient
Δ,δ	difference
ε	random parameter referring to the occupancy rate in optimal control
η	efficiency
θ	dependent variable
λ	thermal conductivity [W/m K]
π	policy
ρ	density [kg/m^3]

Subscripts

ch	charging
comp.	compartments
down	downwards
eq	referred to p as equilibrium
i	referred to x as i-th segment of x
inst	instantaneous
liq	referred to T as liquid
max	maximum
min	minimum
n	referred to t as time step of t
ref	reference
sol	referred to T as solid
up	upwards

Abbreviations

APX	Amsterdam power exchange
BRCM	building resistance-capacitance modeling
BTM	building thermal mass
CHP	combined heat and power
COP	coefficient of performance
DP	dynamic programming
DR	demand response
FD	finite difference
FF	flexibility factor
HP	heat pump
HT	heat transfer
HVAC	heating, ventilation, and air conditioning system
HX	heat exchanger
LDF	linear driving force
OC	optimal control
PCM	phase change material
RC	resistance-capacitance
TCM	thermochemical material
TES	thermal energy storage
TMY	typical meteorological year

information about time periods with constant power but does not consider power variations over time. Based on the work of D'hulst et al. [8] and Reynders et al. [9], Stinner et al. [6] introduce power flexibility using power curves, defined as a time-dependent difference between maximum and reference power. Power flexibility is required to determine flexibility towards power grid stabilization. Recent studies about demand flexibility of buildings suggest costs as an additional dimension of flexibility [4,10]. De Coninck et al. [4] use conventional utility rates, including cost curves, associated with costs of flexibility. In the study of [4], flexibility refers to shifts in the power demand of the heating, ventilation, and air conditioning system (HVAC). Le Dreau et al. [10] suggest the flexibility factor as performance indicator measuring the potential flexibility during operation. The flexibility factor considers variable electricity price periods and indicates whether the controlled system is flexible enough to shift the heating demand from high to low-price periods. An overview of flexibility indicators is given by Clauβ et al. [11]. The review describes performance indicators that relate to all dimensions of demand flexibility. The review also presents an overview of flexibility indicators that are assumed in conventional and modern, optimal control strategies. Clauβ et al. [11] concluded that multiple indicators such as self-consumption, self-generation, flexibility factor, storage capacity, storage efficiency are not yet considered in optimal and model-predictive control.

Potential demand-side flexibility sources have been determined by relevant studies [4–10,12–20]. Electrical power-to-heat and thermal energy storage are identified as effective measures to provide flexibility [12–14,21]. Building-integrated TES technologies are classified into sensible (e.g. building thermal mass (BTM) and water), latent (e.g. phase change materials (PCM) and ice), and thermochemical materials (TCM) [22]. They can also be categorized as active TES (water, ice, PCM, and TCM tanks) and passive TES (BTM and PCM panels) [23,24]. Thermal energy storage can be an effective solution to attune energy supply and demand, combined with electrical appliances. To activate TES tanks with power-to-heat conversion, the working temperature range of the heat storage medium determines the minimum and maximum flexibility. For water tanks, charging and discharging temperatures in space heating (SH) and domestic hot water (DHW) supply is typically between 21 °C and 95 °C [25]. In the case with charging temperatures higher than 95 °C, it is required that the tank equipment can manage high pressures. The use of thermal oil instead of water as storage medium can compensate for higher temperatures but has a comparably lower heat conductivity and specific heat capacity [25]. Adequate materials used as PCM in SH and DHW are presented by Cabeza [26]. The review describes inorganic and organic PCM with melting points up to 120 °C. TCM systems typically hydrate (discharging) above 40 °C and dehydrate (charging) between 80 and 120 °C [27–30]. Latest advances in TCM development include salt hydrates, such as $CaCl_2{\cdot}6H_20$ or $SrBr_2{\cdot}6H_2O$ with dehydration temperatures down

to 52 °C [31]. Furthermore, a regeneration strategy (dehydration) is presented by Mette et al. [32] to enable the dehydration at lower temperatures. The regeneration includes a cascade system in which at least two TCM reactors are required. An experimental case study using zeolite-water as TCM was performed that successfully reduced the dehydration temperature from 180 to 130 °C at similar energy storage capacity [32].

Power-to-heat conversion with heat pumps (HP) is likely the most mature and favorable technology enabling flexibility in smart grid operations. Vanhoudt et al. [15] conducted an experimental study comparing actively controlled heat pumps to common reference installations. By aiming at peak shaving and load shifting due to renewable integration, the study successfully increased self-consumption and decreased grid feed-in. Heat pumps that participate in load matching markets were investigated by Salpakari et al. [14]. A heat pump and water thermal energy storage were successfully integrated into cost-optimal control to provide flexibility for wind and PV integration on an urban level. Considering low-order models for optimal control, the study presented a methodology that can be used as a tool by urban planners to analyze the potential flexibility [14]. Fischer et al. [17] reviewed heat pumps in the context of smart grid integration. The operation of HPs was discussed from a holistic perspective which included typical applied control approaches. Predictive and non-predictive controls were compared and it was concluded that predictive control results in cost optimization but also in an increase in system complexity. Many studies [14,33–36] suggest the application of predictive control and optimal control to enable energy flexibility of HPs with building integrated TES and for prediction of the dynamic behavior of the system and system components. In a study by Berkenkamp et al. [37], dynamics of a water tank were integrated into an optimal control framework to outperform non-predictive control. However, due to computational complexity, low-order linear models were preferred above non-linear water tank models [36,38], PCM tank, and TCM tank models [4,16,39–46]. For water tanks, recent studies include more detailed storage models, such as one-dimensional stratification models [37,47,48] to overcome inaccurate flow and return temperature predictions. This study integrates more detailed TES tank models (water tank, PCM tank, and TCM tank) in an optimal control framework to capture the complex storage dynamics that occur in heat transfer and mass transfer processes. The more detailed storage models are required to comprehensively present the demand flexibility of a building heating system with HP, electric heater, and TES tank.

The main aim of this study is to investigate the demand flexibility of power-to-heat conversion with thermal storage regarding all three dimensions of flexibility; size (energy), time (power) and costs. Flexibility indicators are chosen to represent the energy flexibility (available storage capacity, storage efficiency), the power flexibility (power shifting capability), and flexibility regarding costs (flexibility factor). Additionally, a power flexibility indicator is introduced in this paper. The instantaneous power flexibility shows the potential power flexibility of TES and power-to-heat in any case of charging, discharging or idle mode. The instantaneous power flexibility is a crucial parameter for providing grid ancillary services towards the power grid.

Furthermore, a simulation case study was performed to quantify the chosen flexibility indicators and demand flexibility in both reference and optimal control scenarios. For optimal control, a classical control strategy is chosen using day-ahead electricity prices as a control signal for the scheduling of power-to-heat and TES. Day-ahead and intra-day electricity markets are well-established energy markets aimed at matching energy supply and demand. Given that the flexibility relates to supply and demand-side is not yet considered in electricity markets, making a step towards the electricity markets requires identification and quantification methods for supply flexibility and demand flexibility. The methodology presented in this paper is thus essential. Section 2 describes the methodology and explains the building heating system. In Section 2.1, an overview of models used for the building heating system is provided. In Section 2.2, the models are employed in the framework of reference and optimal control. In Section 2.3, adequate flexibility indicators are explained. Section 3 presents the simulation results and illustrates demand flexibility.

2. Methodology

For the study of demand flexibility of building heating systems, a small-scale office building is assumed that is located in the Netherlands. The building heating demand of a typical winter day in March is determined due to internal gains (lighting, computers, and occupants) and external disturbances (weather conditions). The building heating system is equipped with a heat pump, electric heater, air-blown heat exchanger, and a thermal energy storage tank (Fig. 1).

The heat pump and additional electric heating serve as power-to-heat conversion and the thermal storage tank (water tank, PCM tank, and TCM tank) as the source of flexibility. To investigate and compare the flexibility towards the power grid, reference and optimal control in the building heating system are presented. The reference control assumes a typical feedback controller that uses the heat pump to supply heating. The optimal control integrates the heat pump and optional electric heating with a thermal energy storage tank and aims to optimize the total operational electricity costs. Hourly electricity prices serve as grid signal to optimal control and to optimize flexibility towards the grid. To show the performance of the reference and optimal control scenarios, indicators that relate to demand flexibility are presented.

2.1. Modelling

The models of the building heating system are implemented in a simulation framework using MATLAB2016a. For each model, a simulation time step of 1 s was used to solve equations to limit the truncation error of the TES model.

2.1.1. Heat pump model, air-blown heat exchanger model, and electric heater model

The HP model uses a piecewise-linear interpolation function, including the condenser outlet temperature, the evaporation inlet temperature, and the heating capacity of the heat pump to calculate the

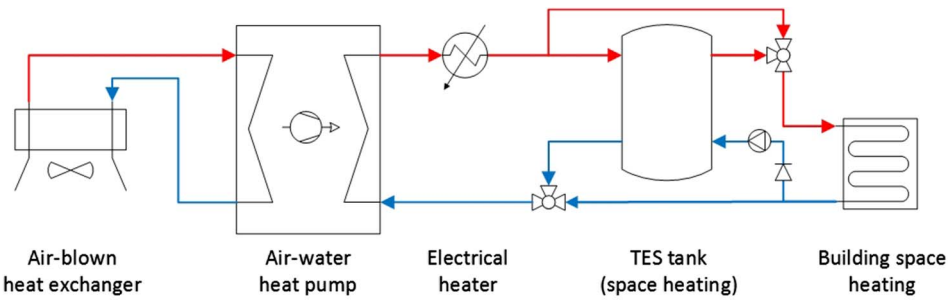

Fig. 1. Simple process flow diagram of building heating system.

coefficient of performance (COP), see Fig. 2. Manufacturer data from Dimplex air-water heat pumps [49] is used to calculate the electrical power consumption and the corresponding COP.

The heat exchanger of the HP on the evaporator side is combined with an air-blown heat exchanger. The model of the air-blown heat exchanger assumes that the evaporator inlet temperature is a constant temperature source equal to the ambient air. The HP provides heating to the building and charges the TES tank. The condenser outlet temperature is considered as the inlet temperature of the radiant heaters and the inlet temperature of the TES tank during charging. The HP guarantees a maximum condenser outlet temperature of 60 °C, sufficiently charging water and PCM tanks. To load TCM tanks, temperatures higher than 60 °C are commonly required to activate the desorption process. In this study, the HP is used to preheat the TCM tank to 60 °C. Auxiliary electric heating provides higher charging temperatures. The model for the electric heater assumes that the heating power is equal to the electrical power consumption.

2.1.2. Building model

A small-scale office building model was adopted from [50] with which the Building Resistance-Capacitance Modeling (BRCM) toolbox [51] was used for building modeling. An advanced resistance-capacitance (RC) network represents the building, including internal and external walls, multiple zones, windows, and the ambient environment. The BRCM toolbox uses constant heat transfer values for conduction in walls, convection, and radiation between walls and zones. The BRCM model has been validated with comparison to EnergyPlus. For this study, the BRCM toolbox was modified to simulate radiant heating by integrating the inlet and outlet temperatures of the radiant heater. A two-floor office building (135 m^2 floor area per floor) with a maximum of eight persons per floor is assumed. [50]. The building consists of 7 rooms per floor and is composed of building elements (Table 1) containing concrete (0.73 W/m K; 921 J/kg K; 1920 kg/m^3) and external mineral insulation (0.04 W/m K; 830 J/kg K; 90 kg/m^3).

2.1.3. Thermal energy storage models

In the models, TES tanks are assumed to be cylindrical vessels. Fig. 3 shows the design of the water tank, PCM tank, and TCM tank.

The water tank is comprised of a vessel without an internal heat exchanger. The PCM and TCM tank include compartments of packed-bed reactors without any additional electric resistance. The number of compartments is a design decision as can be seen in Fig. 4. The dimensions of the heat exchangers include the calculation of the pressure drop which is caused by the flow of the heat transfer medium through the internal heat exchanger of the PCM and TCM tank according to Eq. (1) [52]

$$\Delta p = (V_{dot}, d_{tube,HX}, l_{tube,HX}, Pr, Re, Nu) \tag{1}$$

A PCM tank with four compartments and a TCM tank with eight compartments is chosen.

The PCM and TCM reactors consist of vertical copper tubes covered with the heat storage medium. In the reactor, a layer of heat storage medium (PCM or TCM) is applied to the surface of the copper tubes. Because such a layer may be impractical to add, current setups often make use of finned tubes. However, to simplify the simulation of the PCM and TCM layer, the heat exchanger is modeled with a layer of heat storage material. All TES tanks are insulated using a material 0.1 m thick with a thermal conductivity of 0.033 W/(m K) [53].

Table 1
The building structure of two-floor office building [50].

Building elements	Materials	Thickness [m]
External wall	Mineral insulation; concrete	0.05; 0.30
Internal wall	Concrete	0.15
Ceiling, floor	Concrete	0.25

The heat and mass transfer of the TES tanks is mathematically formulated using a one-dimensional representation. Previous case studies have successfully used the one-dimensional representation of water tanks [54–56], PCM tanks [57,58], and TCM tanks [59,60]. In this case study, the one-dimensional convection-diffusion-reaction equation [61–63] is applied to all TES tanks according to

$$\frac{\partial \theta}{\partial t} = \alpha \frac{\partial^2 \theta}{\partial x^2} - u \frac{\partial \theta}{\partial x} + f(\theta), \quad 0 \leqslant x \leqslant x_{\max}, \quad t \geqslant 0, \tag{2}$$

$$\theta(x,0) = f(x), \quad 0 \leqslant x \leqslant x_{\max}, \tag{2a}$$

$$\theta(0,t) = g(t), \quad 0 \leqslant t \leqslant t_{\max}, \tag{2b}$$

$$\theta(x_{\max},t) = h(t), \quad 0 \leqslant t \leqslant t_{\max}, \tag{2c}$$

where $f(\theta)$ is the reaction term, $\theta = \theta(x,t)$ is the dependent variable, α is a positive constant coefficient, u is a positive constant speed, x is the spatial coordinate, t is time, and $x_{\max}$ is the range of the spatial domain. Here, f(x), g(t) and h(t) are functions that determine the initial conditions (2a) and the boundary conditions (2b), (2c).

The current study applies a finite difference (FD) method to numerically solve the one-dimensional convection-diffusion equation [55,64,65]. The finite difference method uses an approximation to $\theta = \theta(x,t)$ according to

$$\frac{\partial \theta}{\partial x} \approx \frac{\theta_{i+1} - \theta_i}{\Delta x}, \tag{3}$$

$$x_i = (i-1)\Delta x, \quad i = 1,2,...M, \quad 0 \leqslant x \leqslant x_{\max}, \tag{4}$$

$$t_n = (n-1)\Delta t, \quad n = 1,2,...N, \quad 0 \leqslant t \leqslant t_{\max}, \tag{5}$$

where Δx is the spatial discretization and Δt is the temporal discretization [65].

The simulation model integrates the discrete approximation with the implicit and unconditionally stable Crank-Nicolson [66] scheme which is more accurate than other FD-schemes with respect to the temporal truncation error $O(\Delta t^2)$ [65]. The discrete form of Eq. (2) is calculated according to

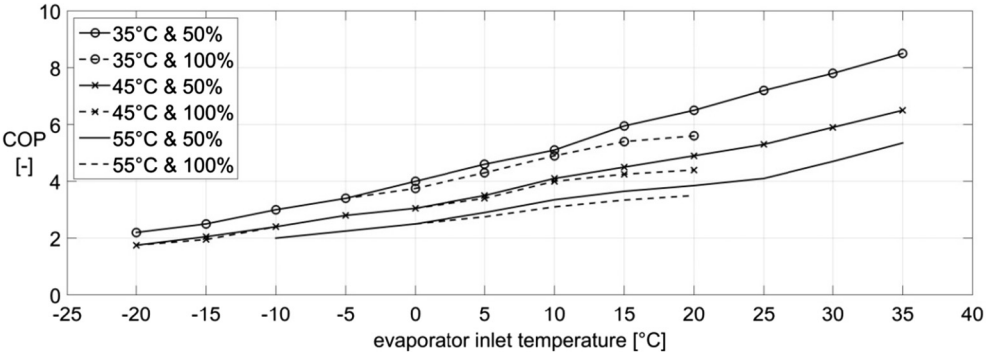

Fig. 2. Performance of the air-water heat pump (HP). The coefficient of performance (COP) is a function of evaporator inlet temperature for different condenser outlet temperatures (35 °C, 45 °C, 55 °C) and heating capacity of the heat pump (50%, 100%) [49].

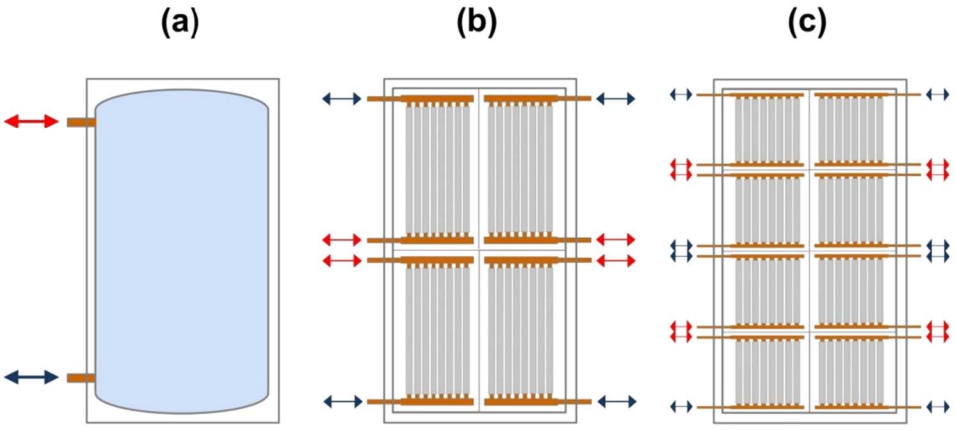

Fig. 3. Schematic design of thermal energy storage (TES) tanks: (a) water tank; (b) packed-bed phased change material (PCM) tank with four compartments; (c) packed-bed thermochemical material (TCM) tank with eight compartments.

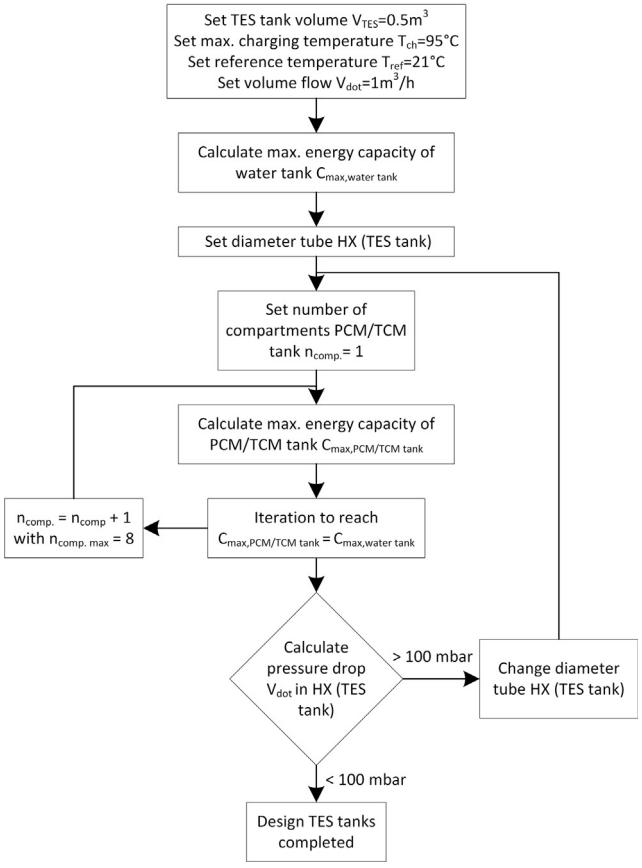

Fig. 4. Flowchart design decision of TES tanks.

$$\alpha\frac{\partial^2\theta}{\partial x^2} = \frac{\alpha}{2}\left(\frac{\theta_{i+1}^{n+1}-2\theta_i^{n+1}+\theta_{i-1}^{n+1}}{\Delta x^2} + \frac{\theta_{i+1}^{n}-2\theta_i^{n}+\theta_{i-1}^{n}}{\Delta x^2}\right) \tag{6}$$

$$a\frac{\partial\theta}{\partial x} = \frac{u}{4}\left(\frac{\theta_{i+1}^{n+1}-\theta_{i-1}^{n+1}+\theta_{i+1}^{n}-\theta_{i-1}^{n}}{\Delta x}\right). \tag{7}$$

The convection-diffusion equation can now be written as

$$\frac{\theta_i^{n+1}-\theta_i^n}{\Delta t} = \frac{\alpha}{2}\left(\frac{\theta_{i+1}^{n+1}-2\theta_i^{n+1}+\theta_{i-1}^{n+1}}{\Delta x^2} + \frac{\theta_{i+1}^{n}-2\theta_i^{n}+\theta_{i-1}^{n}}{\Delta x^2}\right) - \frac{u}{4}\left(\frac{\theta_{i+1}^{n+1}-\theta_{i-1}^{n+1}+\theta_{i+1}^{n}-\theta_{i-1}^{n}}{\Delta x}\right) + f(\theta_i^n). \tag{8}$$

In the following sections, this approach is applied to the water tank, PCM tank, and TCM tank. The main heat and mass transfer effects and their implementations in the numerical solution are described.

2.1.4. Water tank model

The model uses a stratified water tank. For charging, inflow takes place at the top, and outflow at the bottom. In the case of discharging, i.e. providing heating, cold water enters the bottom and leaves through the top (see Fig. 3). The model includes heat and mass transfer by convection and conduction. A vertical temperature distribution $\partial T/\partial x$ is assumed which depends on the speed of the water flow u and the thermal properties to obtain α according to

$$\frac{\partial T}{\partial t} = \alpha\frac{\partial^2 T}{\partial x^2} - u\frac{\partial T}{\partial x}, \quad 0 \leqslant x \leqslant x_{\max}, \quad t \geqslant 0 \tag{9}$$

$$\alpha = \frac{\lambda}{\rho c_p}, \tag{10}$$

where x is the spatial vertical coordinate and $x_{\max}$ is the height of the tank. The speed u is spatially constant and derived from the water volume flow divided by the cross sectional area perpendicular to the volume flow. Table 2 shows the properties of the water tank and the water as a heat transfer and storage medium.

2.1.5. Phase change material tank model

The water enters the PCM tank and exchanges heat with the PCM layer (Fig. 3) which melts during charging and, to provide heating, solidifies during discharging. The model uses the enthalpy h of the PCM to implement the melting process in the model. Eq. (11) shows a one-dimensional formulation for the PCM including heat conduction through the PCM layer [58] according to

$$\rho\frac{\partial h}{\partial t} = \lambda\frac{\partial^2 T}{\partial x^2}, \quad 0 \leqslant x \leqslant x_{\max}, \quad t \geqslant 0, \tag{11}$$

in which x is the spatial coordinate and $x_{\max}$ the thickness of the PCM layer. Table 3 presents the properties of the PCM tank. The design of the PCM tank is adapted to the volume and energy capacity of the water tank according to Fig. 4.

Table 4 presents the properties of the PCM. $CaCl_2{\cdot}6H_2O$ was chosen as PCM because it melts at 29 °C that is below typical maximum charging temperatures of heat pumps of 60 °C. An overview of PCMs for heat storage application with different melting points can be found in [26,67,68].

The enthalpy formulation (Eq. (11)) enables the implementation of

Table 2
Properties of water as heat storage and heat transfer medium.

Water tank volume [m³]	Volume flow [m³/h]	Density [kg/m³] (303 K)	Specific heat [J/kg K] (303 K)	Thermal conductivity [W/m K] (303 K)	Max. energy capacity [GJ] deltaT = 74 K
0.5	1	996	4180	0.616	0.15

Table 3
Properties of the PCM tank.

PCM tank volume [m³]	Number of compart. [−]	Volume flow of heat transfer medium [m³/h]	Diameter of heat exchanger tube [m]	Length of heat exchanger tube per compart. [m]	Thickness of PCM layer [m]	Mass of PCM [kg]	Max. energy capacity [GJ] deltaT = 74 K
0.5	4	1	0.025	35	0.015	511	0.15

Table 4
Properties of the PCM ($CaCl_2{\cdot}6H_2O$) [69].

Melting point [°C]	Melting enthalpy [J/kg]	Density [kg/m³]		Specific heat [J/kg K]		Thermal conductivity [W/m K]	
		Solid	Liquid	Solid	Liquid	Solid	Liquid
29	190.8e03	1710	1530	2200	1400	1.09	0.54

non-isothermal phase change. Fig. 5 illustrates the relationship between enthalpy and temperature, highlighting the transition phase between the solid and liquid state of the PCM.

Non-isothermal phase change is calculated according to [58]

$$h = \begin{cases} c_{p,sol}\,T & T \leqslant T_{sol} \\ c_{p,sol}\,T_{sol} + \frac{h_{\Delta liq,sol}\,(T - T_{sol})}{(T_{liq} - T_{sol})} & T_{sol} < T \leqslant T_{liq} \\ c_{p,sol}\,T_{sol} + h_{\Delta liq,sol} + c_{p,liq}\,T & T > T_{liq} \end{cases} \tag{12}$$

Furthermore, to simplify the simulations, it is assumed that the PCM is homogenous and isotropic [69] and natural heat convection during the melting process is neglected [70].

2.1.6. Thermochemical material tank model

The model uses a closed TCM unit consisting of the sorption unit (TCM tank) and an evaporator-condenser unit and operates in a vacuum. The TCM tank is a packed-bed reactor in which a sorbent (zeolite13X) desorbs and adsorbs a fluid (water). During desorption, a high-temperature source such as an electric heater serves as a dehydration source. A condenser that is supplied by a low-temperature source, such as ambient air, collects the produced refrigerant (water). During adsorption, the condenser operates as an evaporator. The refrigerant is evaporated and simultaneously adsorbed. The released heat from the TCM tank can be used for space heating or domestic hot water [29,71]. This study uses zeolite13X-water as a sorption pair because it is one of the most common TCM in current research on component and system design with favorable hydrothermal and mechanical stability and corrosion behavior [29]. The latest advances in TCM development focus on salt hydrates, such as $Na_2S{\cdot}9H_2O$ with an energy density of up to 3.17 GJ/m³ [72].

The TCM tank model is similar to the PCM tank model (Fig. 3), but the PCM is replaced by a TCM as the heat storage medium. The evaporator and condenser are assumed to be a constant, low-temperature source. Additional heat exchange for the process of evaporation and condensation is not modeled.

The heat and mass transfer model of the TCM unit includes the diffusion of the refrigerant (water) to and through the adsorbent (zeolite13X), the adsorption process, the heat conduction through the TCM layer, and heat exchange with the heat transfer medium [59,73]. Heat transfer in the adsorbent bed is calculated by

$$\frac{\partial T}{\partial t} = \alpha\frac{\partial^2 T}{\partial x^2} + \frac{Q_s}{c_p}\frac{d\bar{q}}{dt}, \quad 0 \leqslant x \leqslant x_{\max}, \quad t \geqslant 0, \tag{13}$$

moreover, the mass diffusion process through the adsorbent bed is calculated with

$$\frac{\partial m_{ads}}{\partial t} = D\frac{\partial^2 m_{ads}}{\partial x^2} + m_{sorb}\frac{d\bar{q}}{dt}, \quad 0 \leqslant x \leqslant x_{\max}, \quad t \geqslant 0, \tag{14}$$

where x is the spatial coordinate, $x_{\max}$ is the thickness of the TCM layer, and m_{sorb} is the mass of the dry adsorbent. Here, $T = T(x,t)$ describes the temperature distribution affected by the rate of adsorbed refrigerant $d\bar{q}$ and the adsorption enthalpy Q_s. $m_{ads} = m_{ads}(x,t)$ represents the adsorbate distribution in the TCM layer affected by the diffusion D of the refrigerant through the adsorbent [59,73]. The average rate of adsorbed refrigerant $d\bar{q}$ is the main driving force during the adsorption process and implemented using the linear driving force (LDF) method according to

$$\frac{d\bar{q}}{dt} = k_m(q_{eq} - \bar{q}). \tag{15}$$

The LDF method accounts for the difference between equilibrium and amount of adsorbate including the mass transfer coefficient k_m [59,73]. This linear driving force is determined by calculating the vapor pressure of water in equilibrium and in solid phase of the dry material (zeolite13X). The equilibrium vapor pressure relates to the condensation and evaporation temperature, because condensation and evaporation model are considered as constant temperature source. The vapor pressure values in equilibrium and in solid phase of the dry material are derived from the Clausius-Clapeyron relation [71] according to

$$\frac{dp}{dT} = \frac{\Delta h_v}{T\Delta v} \cong \frac{p\Delta h_v}{RT^2}, \tag{16}$$

in which Δh_v is the molar enthalpy, Δv is the molar volume difference of water vapor (also illustrated in Fig. 6).

Tables 5 and 6 show the properties of the TCM tank and the TCM layer. The design of the TCM tank is adapted to the volume of the water and PCM tank according to Fig. 4. The energy capacity is 1/3 compared with the water and PCM tank. To reach a larger energy capacity higher charging temperatures than 95 °C are required. Alternatively, a different TCM material can be chosen. However, this study considers zeolite13X-water because all the material properties (Table 6) are available.

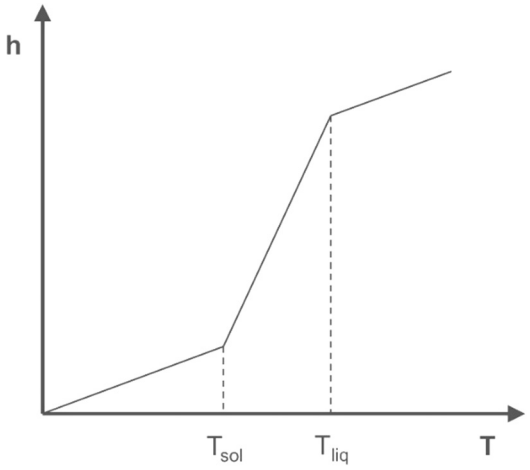

Fig. 5. Piecewise-linear function h(T) for non-isothermal phase change with the transition temperature Tsol between the solid and solid-liquid interface and the transition temperature Tliq between the liquid and solid-liquid interface [58].

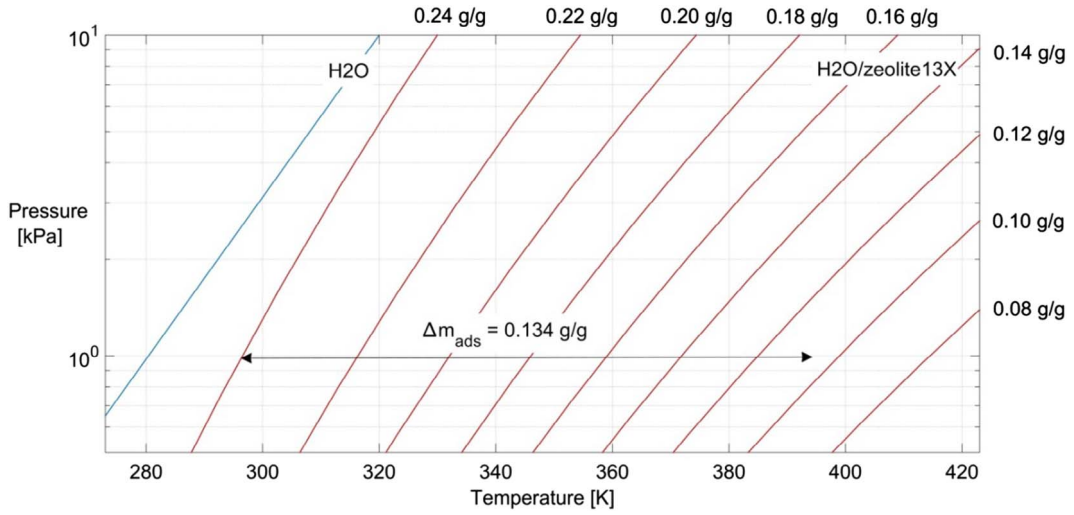

Fig. 6. Vapor pressure lines for zeolite 13X–water based on data from [74] with a maximum capacity of 0.24 g/g [75]. Desorption temperature at 120 °C, condensation and evaporation temperature at 10 °C, and adsorption temperature at 20 °C result in a loading difference of 0.134 g/g.

2.2. Control framework

The models of the building heating system are implemented in the framework of reference control, and optimal control and simulations are conducted for the different TES tanks.

2.2.1. Reference control

In the reference control, the HP is used to compensate the heating demand of the building. To identify maximum flexibility, TES tanks are not applied in the reference case. Due to the absence of TES, optimization is not required and a feedback controller (P-controller) is implemented to investigate reference control. The feedback controller regulates the heat pump based on predefined temperature set points $T_{zone,set}$ according to:

$$T_{zone,set} = \begin{Bmatrix} 15°C, & t = 0{-}6{,}19{-}24 \\ 15°C, & t = 6{-}7 \\ 20°C, & t = 7{-}8{,}12{-}13{,}17{-}19 \\ 21.5°C, & t = 8{-}12{,}13{-}17 \end{Bmatrix} \quad (17)$$

To limit the start-stop cycles of the HP to a maximum of four times per hour, a control time step of 15 min is used. The electricity consumption of the air-blown heat exchanger is not considered.

2.2.2. Optimal control

The optimal control of the building heating system aims to minimize the electricity consumption costs for operating the HP and the electric heater. The control time step of 15 min is identical to reference control. The electricity consumption of the air-blown heat exchanger is as introduced not considered. The cost-optimal control schedules the charging and discharging of either the water tank, the PCM tank, or the TCM tank, by making use of a dynamic optimization routine to predict control actions for 24 h. Fig. 7 shows the framework of the optimal control of the building heating system including grid signal, constraints, disturbances, objective function, optimization problem, state variables, and control variables. The grid signal corresponds to hourly day-ahead electricity prices that are taken from the Dutch Amsterdam Power Exchange (APX) power spot market for an average day in March 2016 during the heating period. Disturbances in optimal control estimate internal heating gains and ambient conditions. The occupancy rate ϵ_t is used to model the internal heat gains of lighting systems, computers, and occupants. The occupancy rate refers to the ratio of occupants to the maximum amount of occupants and determines the minimum comfort temperature $T_{zone,\min}$ according to:

$$\epsilon_t = \begin{Bmatrix} 0, & T_{zone,\min} = 15°C, & t = 0{-}6{,}19{-}24 \\ 0.1, & T_{zone,\min} = 15°C, & t = 6{-}7 \\ 0.5, & T_{zone,\min} = 20°C, & t = 7{-}8{,}12{-}13{,}17{-}19 \\ >0.7, & T_{zone,\min} = 21.5°C, & t = 8{-}12{,}13{-}17 \end{Bmatrix} \quad (18)$$

The occupancy model, which allows the implementation of Markov chains, is adopted from [77]. More information about the occupancy model can be found in a previous case study [50]. However, in this case study, perfect occupancy prediction and ideal weather forecasting are assumed. Fig. 8 presents the weather data from a small-scale office building located in the Netherlands.

The optimal control framework uses the TES tank models integrated with the building heating system as discussed in Section 2.1. Because the building heating system including TES tanks is inherently nonlinear, the optimal control problem is solved using dynamic programming (DP) as optimization methodology. Dynamic programming employs the different TES tank models for reasonable computation times. The basic structure of dynamic programming refers to the Bellman equation [78] according to,

Table 6
Properties of the TCM (zeolite13X-water) [75,76].

Adsorption enthalpy [J/kg]	Density [kg/m^3]	Specific heat [J/kg K]	Thermal conductivity [W/m K]	Diffusion coefficient [m^2/s]
3.2e06	620	836	0.2	7.5e-09

Table 5
Properties of TCM tank.

TCM tank volume [m^3]	Number of compart. [−]	Volume flow of heat transfer medium [m^3/h]	Diameter of heat exchanger tube [m]	Length of heat exchanger tube per compart. [m]	Thickness of TCM layer [m]	Mass of TCM [kg]	Energy capacity [GJ] deltaT = 74 K
0.5	8	1	0.025	45	0.005	122	0.05

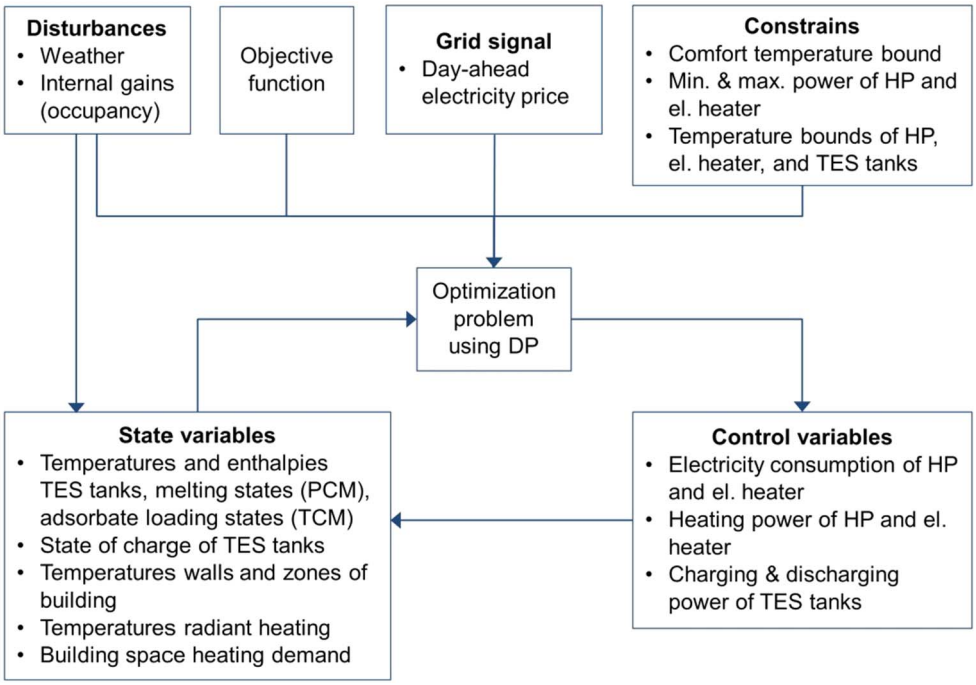

Fig. 7. Framework of optimal control of building heating system.

$$J(x_0) = \min_\pi J_\pi(x_0) \tag{19}$$

$$J_\pi(x_0) = E\left[g_N(x_N) + \sum_{t=0}^{N} (x_t,\mu_t(x_t),\varepsilon_t)\right] \tag{20}$$

$$x_{t+1} = f_t(x_t,u_t,\varepsilon_t), \quad t = 0,\ldots,N-1 \tag{21}$$

$$\text{with} \quad u_t \in U_t(x_t), \quad \pi = \{\mu_0,\ldots,\mu_{N-1}\}, \quad u_t = \mu_t(x_t), \quad \mu_t(x_t) \in U_t(x_t) \;\forall\; x_t \tag{21a}$$

where f_t describes the building heating system, t the discrete time, N the planning horizon of 24 h, x_t the state variables, u_t the controls variables, U_t the control constraints, ε_t the random parameter (occupancy rate), $J(x_0)$ the optimal cost function, and $J_\pi(x_0)$ the expected costs with the policy π at x_0. Because dynamic programming aims to minimize the electricity consumption costs for operating the HP and the electric heater, the objective function to be minimized consists of the total expected costs for electricity usage. As can be seen in Fig. 7, the control variables are associated with power consumption and heating power of the HP and electric heater, and the charging and discharging power of the TES tank. DP employs these control options having a vector of discrete states in which:

- HP compensates heating demand of building (no charging and discharging of TES)
- HP compensates heating demand of building and charges TES tank, optionally additional charging of TES tank by electric heating
- HP and discharge of TES compensate heating demand of building
- HP and optionally electric heater charge TES tank (no heating demand of building)

The control options are implemented in the DP loop as control decisions which are calculated at each state as can be seen in Fig. 9.

2.3. Demand flexibility

Cost-optimal control applies day-ahead electricity prices as grid signal that is crucial information for the optimization. Besides, the forecasting of weather, the predictions of internal heating gains, and the design of the heating system determine the optimal use of building demand flexibility. The amount of flexibility a building heating system can deliver regarding all three dimensions of demand flexibility, size (energy), time (power) and costs, is quantified in corresponding flexibility indicators.

2.3.1. Demand flexibility – energy

In this case study, the indicators, available storage capacity, storage efficiency [18] represent the energy flexibility. Eq. (22) shows the available storage capacity according to

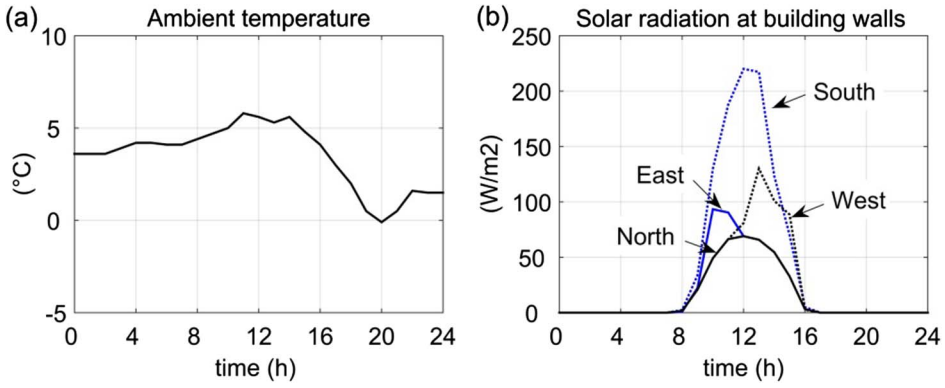

Fig. 8. Typical meteorological year (TMY) weather data for De Bilt, the Netherlands, 1st of March: (a) ambient temperature, (b) solar radiation at building walls.

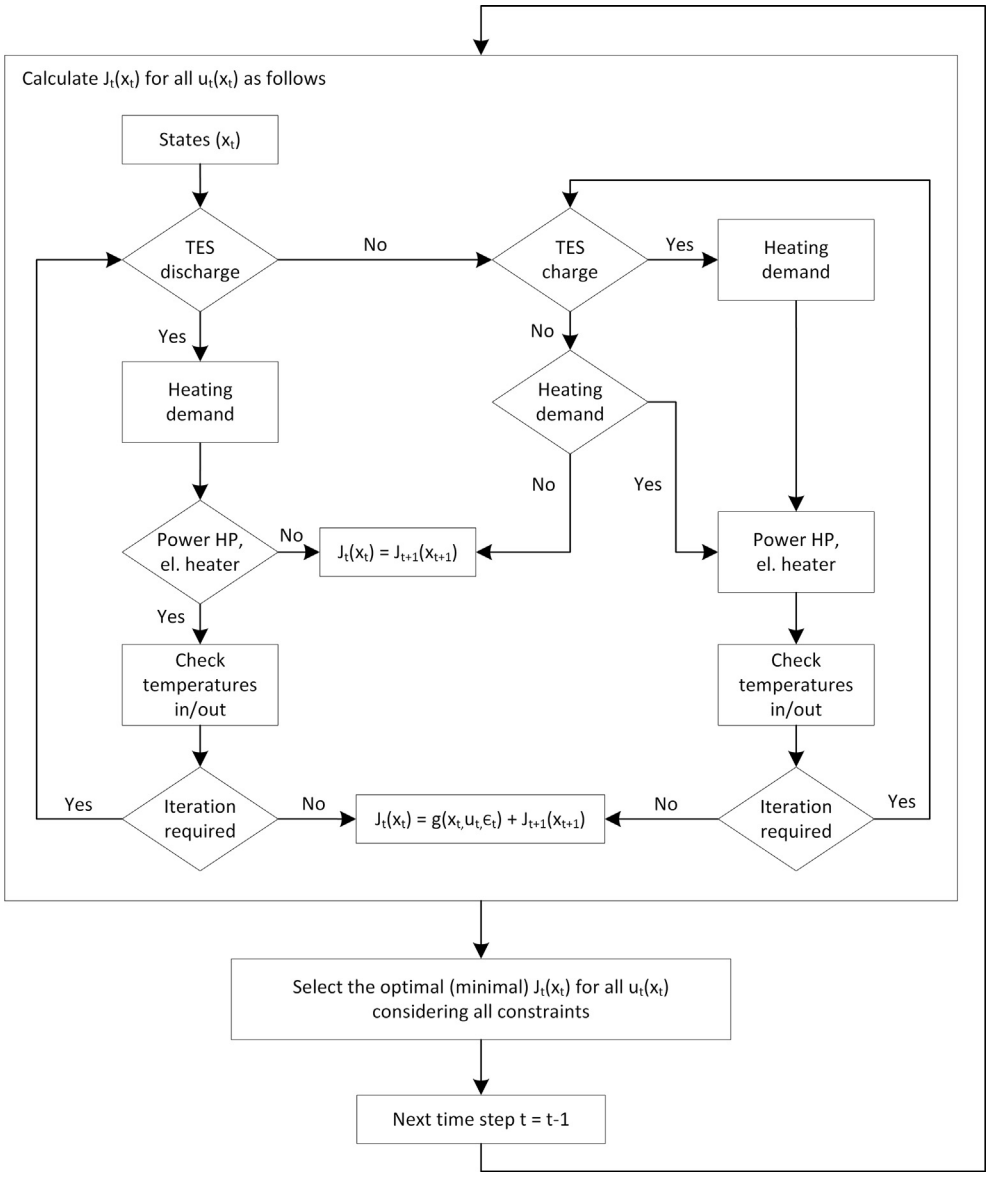

Fig. 9. Simplified flowchart of control decisions at each state in dynamic programming (DP) optimization loop.

$$C_{OC} = \int_0^{l_{OC}} (Q_{OC} - Q_{Ref})\,dt \tag{22}$$

where C_{OC} is the available storage capacity, Q_{OC} the heating power, and l_{OC} the duration corresponding to the period of optimal control (OC). The heating demand during reference control is formulated as Q_{Ref} [18]. The available storage capacity can be summarized as the amount of energy that is shifted during optimal control. In cost-optimal control, charging and discharging of a TES tank takes place in a control horizon of 24 h. While charging events refer to demand increase as upward storage capacity $C_{OC,up}$, discharging events represent demand decrease as downward storage capacity $C_{OC,down}$. The ratio between discharging and charging events over the entire 24 h control horizon is defined as storage efficiency [18] or shifting efficiency [10] η_{OC}. According to Eq. (23),

$$\eta_{OC} = \frac{\sum_{n_{OC}=1}^{m} \int_0^{l_{OC,down}} (Q_{OC,down} - Q_{Ref})\,dt}{\sum_{n_{OC}=1}^{m} \int_0^{l_{OC,up}} (Q_{OC,up} - Q_{Ref})\,dt} \tag{23}$$

The storage efficiency indicates the effective use of the stored heat that compensates HP heating power during optimal control.

2.3.2. Demand flexibility – costs

An energy flexibility indicator that relates to the dimension of electricity costs during operation is the flexibility factor FF [10]. Low electricity and high electricity periods are considered according to

$$FF = \frac{\int_0^{l_{lowprice}} Q_{heating}\,dt - \int_0^{l_{highprice}} Q_{heating}\,dt}{\int_0^{l_{lowprice}} Q_{heating}\,dt + \int_0^{l_{highprice}} Q_{heating}\,dt} \tag{24}$$

In which $Q_{heating}$ is the amount of heating power over low and high-price periods l. To estimate the different pricing periods, standard deviation is assumed that relates to the electricity prices of the entire 24 h control horizon. Pricing periods that exceed the normal distribution with one standard deviation of -1σ and 1σ account for either low and high price periods. The flexibility factor varies between -1 and 1 whereas -1 correlates to a highly inflexible controlled system and 1 indicates highest desired flexibility.

2.3.3. Demand flexibility – power

Energy flexibility is introduced as the integral of power flexibility which refers to the evolution of heating power during each time step of optimal control. An indicator of power flexibility is the power shifting capability [18] according to

$$Q_{\delta} = Q_{OC} - Q_{Ref} \quad (25)$$

where Q_{δ} is the difference between power consumption during optimal control and reference control. For a building heating system with HP, electric heater and TES, the power shifting capability includes thermal (heating) power shifting $Q_{\delta,th}$ according to

$$Q_{\delta,th} = (Q_{OC,th.output\ HP} + Q_{OC,th.outputel.heater}) - (Q_{Ref,th.output\ HP} + Q_{Ref,th.outputel.heater}) \quad (26)$$

and electrical power shifting $Q_{\delta,el}$ due to the electricity consumption of the HP and electric heater.

$$Q_{\delta,el} = (Q_{OC,el.cons.HP} + Q_{OC,el.cons.el.heater}) - (Q_{Ref,el.cons.HP} + Q_{Ref,el.cons.el.heater}) \quad (27)$$

To comprehensively represent the potential power flexibility of TES and power-to-heat, this paper introduces the instantaneous power flexibility. In contrast to the power shifting capability, the instantaneous power flexibility does not require the determination of a reference case and represents the potential flexibility towards the power grid. This is crucial information to provide grid ancillary services of very short (1 ms – 5 min), short (5 min – 1 h), intermediate (1 h – 3 d) and long duration (> 3 d) [12]. Because TES systems mostly slowly respond to variations, services to the electricity grid and power market as of 5 min time scale are suitable. Possible services relate to electricity spot markets and load shaping, leveling, peak reduction and congestion management [12,17]. In this case study, the instantaneous power flexibility Q_{inst} is presented on a flexibility time step of 1 h and includes electrical instantaneous power flexibility according to

$$Q_{inst.el.} = f(Q_{inst.th.}, COP_{power-to-heat}), \quad (28)$$

and thermal instantaneous power flexibility according to

$$Q_{inst.th.} = f(T_{HT}, \dot{m}_{HT}), \quad (29)$$

where T_{HT} is the temperature, and $\dot{m}_{HT}$ is the mass flow of the heat transfer medium that are used to charge or discharge the TES tank. In any case of charging, discharging or idle mode, the instantaneous power flexibility shows the thermal response of TES tanks and the electrical response of power-to-heat devices. The presentation of the thermal response of TES is introduced as performance maps of TES [79]. These maps are developed to show the dynamic behavior of TES in the control of building energy systems. An example of performance maps of the PCM tank is illustrated in Fig. 10 and takes into account the properties presented in Section 2.1.3.

In this case study, the performance maps of TES tanks are used to calculate the thermal instantaneous power flexibility. As an example, a charging case is simulated in which the TES tanks are charged with a temperature of 95 °C. Based on the control decisions of cost-optimal control, the thermal and electrical instantaneous power flexibility are simulated for each optimal control time step. The thermal response of TES tanks and the electrical response of power-to-heat devices is shown for a flexibility time step of 1 h. It is to emphasize that the flexibility time step of 1 h is calculated with intermediate steps of 5 min to exclude any starting effects of the first 5 min.

3. Simulation results

3.1. Reference control

In reference control, the HP compensates the heating demand of the building. As described in Section 2.2.1, TES tanks are not considered in the reference case. Fig. 11 shows the simulation results of the reference control with 15 min control time steps.

The building heating consumption (Fig. 11a) is identical to the heating supplied by the HP (Fig. 11b). The resulting average COP is 4.5. As can be seen in Fig. 11c the average indoor temperature (zones) is always maintained above the minimum zone temperature set points (Eq. (17)). When the heating power is reduced or heating supply is switched off, the zone temperature drops. For example, between 5 pm and 6 pm, the zone temperature decreases from 21.5 °C to 20 °C. This is due to the lower temperatures of the internal (Int. wall) and external

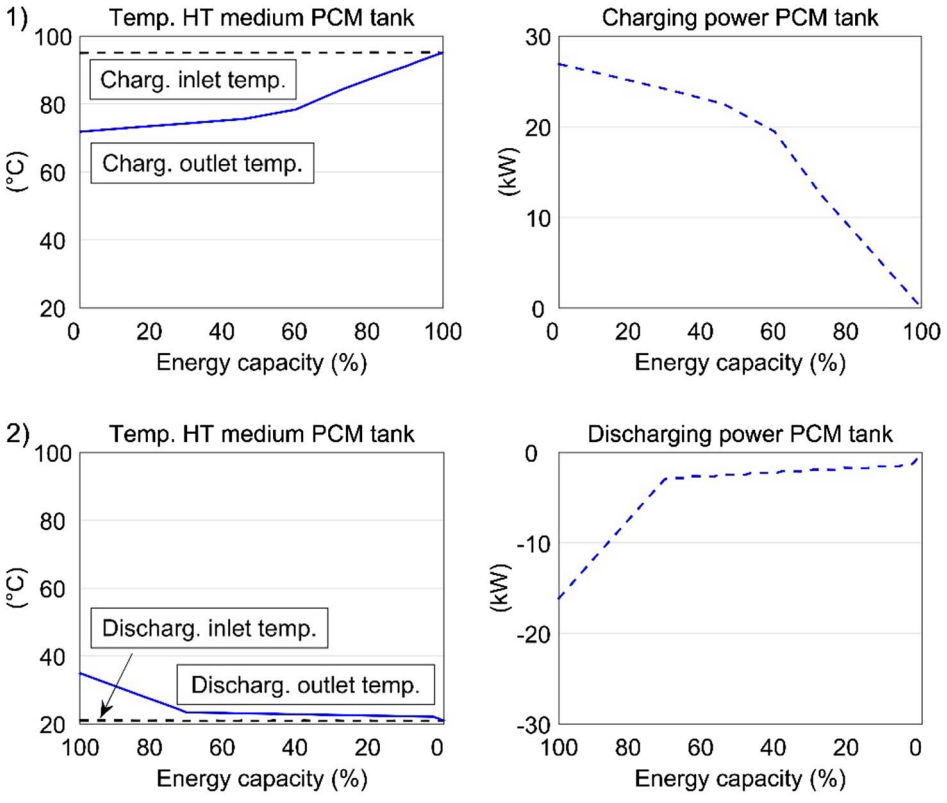

Fig. 10. Performance maps of the PCM tank. The performance maps show inlet, outlet temperature of the heat transfer (HT) medium over energy capacity and charging/discharging power over energy capacity [79]. The properties of the PCM tank are taken from Section 2.1.3. The performance maps are illustrated for 1) a charging case in which the PCM tank is charged from 0% (21 °C) to 100% (95 °C), 2) a discharging case in which the PCM tank is discharged from 100% (95 °C) to 0% (21 °C).

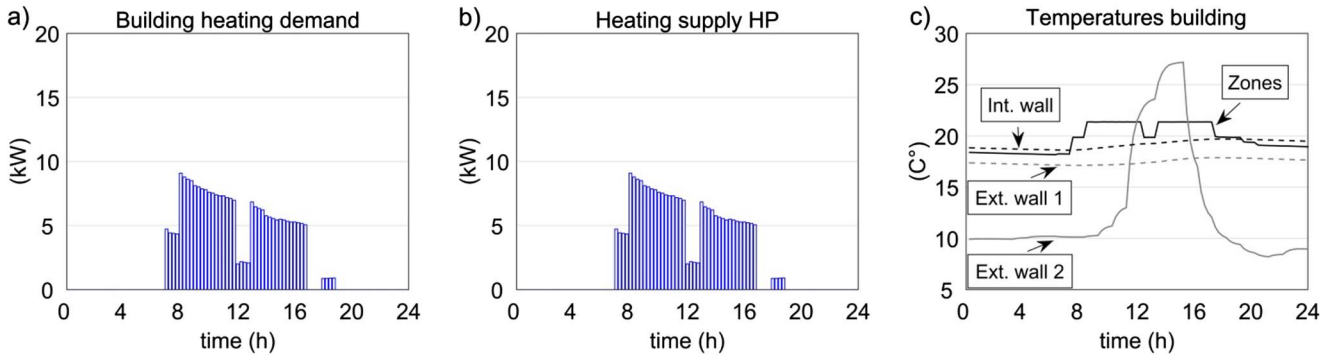

Fig. 11. Simulation results – reference control, a) building heating consumption, b) heating supply by the HP, and c) temperatures in building including average indoor temperature (zones), average temperature of the concrete of the internal walls (Int. wall), average temperature of the concrete at the inner surface of the external walls (Ext. wall 1), and average temperature of the insulation at the outer surface of the external walls (Ext. wall 2).

walls (Ext. wall 1) (Fig. 11c).

3.2. Optimal control

In optimal control, HP and TES are used to compensate the heating demand of the building. The heating consumption is similar to the reference case. In contrast to reference control, optimal control applies the use of TES tanks including optimization of charging and discharging. As introduced in Section 2.2.2, optimal operation of TES, HP and electric heater account for minimizing the total operational electricity costs that correspond to hourly APX electricity prices (Fig. 12).

APX prices serve as main grid signal enabling flexibility in the context of cost-optimal control. Fig. 13 illustrates the simulation results of optimal control with charging and discharging profiles of the water tank, PCM tank, and TCM tank.

It is clear from the nature of optimization that charging the TES tanks takes place when electricity prices are low (2 am – 6 am) whereas discharging is favored when electricity prices are high (7 am – 9 am). The optimization results show that the TES tanks are charged by the HP only, and no additional electric heating is applied to further increase the charging temperature. Essentially for this particular day, this means that an electric heater with a COP of 1 does not compensate any heating power in high price periods. It can be seen in Fig. 13 that implementing a water tank achieves highest average charging (+) and discharging (−) power of +7.5 kW and −6.2 kW. It is observed that during some periods of high charging, the maximum thermal output of the HP of 13 kW limits the charging of the water tank. This effect is not observed for the PCM and TCM tank. Compared to the reference case (1.41 €), the water tank achieves highest total operational electricity cost savings of 7.1 % (1.31 €), the PCM tank 6.4 % (1.32 €), and the TCM tank 2.9 % (1.37 €). The average COP marginally deviates from the reference case with 4.6 (water tank), 4.5 (PCM tank), and 4.6 (TCM tank). As can be seen in Fig. 13c the average temperature of the zones is always maintained above the minimum zone temperature set points (Eq. (18)).

3.3. Demand flexibility

3.3.1. Demand flexibility – energy

Optimal control achieves cost savings and enables energy flexibility. The results of adequate energy flexibility indicators for the different TES tanks are listed in Table 7.

The available storage capacity obtains largest values for the water tank. The storage efficiency is almost similar for all the different technologies. The storage efficiency presents the ratio between discharging and charging for the entire control horizon including heat losses. It is to emphasize that the heat losses are low for all TES tanks and < 1% of storage efficiency.

3.3.2. Demand flexibility – costs

The flexibility factor as indicator of flexibility in the dimension of operational costs refers to high and low-price periods. The standard deviation of the daily electricity price serves to determine the high-price periods (Fig. 14a) and low-price periods (Fig. 14b). The corresponding flexibility factor is calculated and can be seen in Fig. 14c. In the reference control, electricity consumption occurs during high price periods which results in a flexibility factor of -1 that is a highly inflexible controlled system. By adding TES tanks and cost-optimal control, the flexibility factor can be increased to 0.15 (TCM tank), 0.67 (PCM tank), and 0.86 (water tank).

3.3.3. Demand flexibility – power

The power shifting capability determines the power flexibility in optimal control compared with reference control. The power shifting capability is illustrated in Fig. 15 indicating the thermal (TES) and electrical (HP) power flexibility. Because optimal control does not result in operations of electric heating, the electric heater is not considered in Fig. 15.

Optimal control of a water tank achieves highest power shifting capability which is identical to the results shown in Fig. 13-1a) in which the integral of the power flexibility is shown. However, the power shifting capability as shown in Fig. 15 reveals the detailed dynamic response of the TES. For the water tank, variations of up to 9 kW (one-minute average) during a 15 min control time step of charging and discharging power appear that is due to previous scheduling. It can also be seen that stratification is not established during periods of alternating charging and discharging such as between 13 pm and 15 pm. The PCM tank provides almost constant charging and discharging power during the 15 min control time step that is due to the phase change process in which the PCM gradually melts or solidifies. For the TCM tank, charging and discharging variations during the 15 min time step are the highest among the TES tanks of up to 10 kW (one-minute

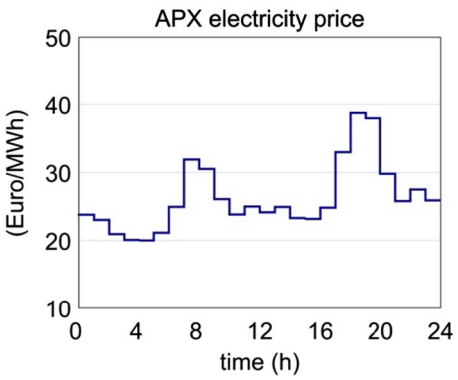

Fig. 12. Amsterdam Power Exchange (APX) electricity prices from 01.03.2016.

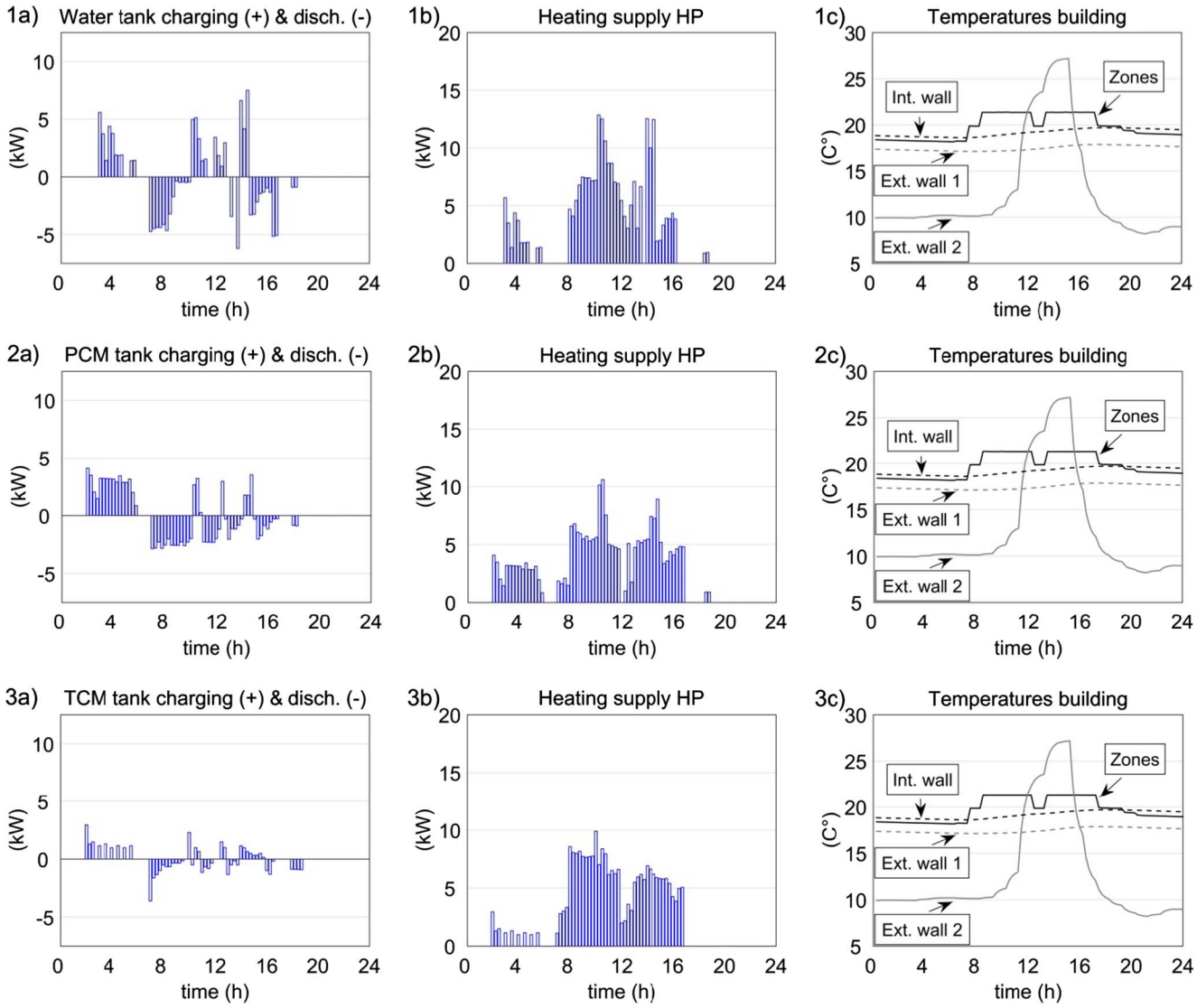

Fig. 13. Simulation results – optimal control including TES tanks 1) water tank, 2) PCM tank, 3) TCM tank, a) charging and discharging power, b) heating supply by the HP, and c) temperature in building including average indoor temperature (zones), average temperature of the concrete of the internal walls (Int. wall), average temperature of the concrete at the inner surface of the external walls (Ext. wall 1), and average temperature of the insulation at the outer surface of the external walls (Ext. wall 2).

Table 7
Simulation results – energy flexibility of different TES tanks comparing optimal control with reference control: available storage capacity C_{ADR} and storage efficiency η_{ADR}.

Energy flexibility indicators	Water tank	PCM tank	TCM tank
$C_{ADR,up}$ [kW h]	17.8	15.3	5.9
$C_{ADR,down}$ [kW h]	17.3	14.8	5.6
η_{ADR} [−]	0.98	0.97	0.96

average). This is because the TCM tank is primarily used as sensible heat storage in which the material quickly heats up and cools down during low activation temperature during charging, the proportion of chemical to sensible heat stored is low.

To identify the full flexibility potential of TES and power-to-heat, the instantaneous power flexibility is introduced which gives an insight into the potential power flexibility provided to the power grid (Fig. 16).

The instantaneous power flexibility presents the thermal response of TES tanks and related electricity consumption of the HP during charging, discharging and rest mode. In this case study, the instantaneous power flexibility is calculated for charging of 95 °C for one hour and illustrated in Fig. 16. The simulation results of cost-optimal control serve as an initial condition to determine the instantaneous power flexibility, once cost-optimal control decision is taken but not applied yet. Knowing all information about the instantaneous power flexibility may result in a new control decision. However, it can be seen that the water tank provides the largest thermal instantaneous power flexibility. For example after 12 h of control horizon, charging with 95 °C gives a thermal power that can sustain between 86 and 67 kW for 25 min of flexibility time step. Adequate electrical instantaneous power flexibility of heat pump and electric heater power varies between 57 and 44 kW. At 12 am the water tank can be charged from 12% to 100% of energy capacity after about 45 min of flexibility time step regarding a charging temperature of 95 °C and a reference temperature of 21 °C. The change from 12% to 100% correlates to an energy uptake of about 0.13 GJ. During the entire control horizon of 24 h, it can be seen that the water tank can always be charged with high power. This indicates that for this particular day, optimal control of a water tank only partly uses the available energy capacity. For the PCM, the same results are observed. At each time step of the entire control horizon of 24 h, the PCM tank can serve as a relatively constant thermal charging source. For example at 12 am the thermal power can sustain between 27 and 21 kW for 60 min of flexibility time step. Due to the high charging temperature of

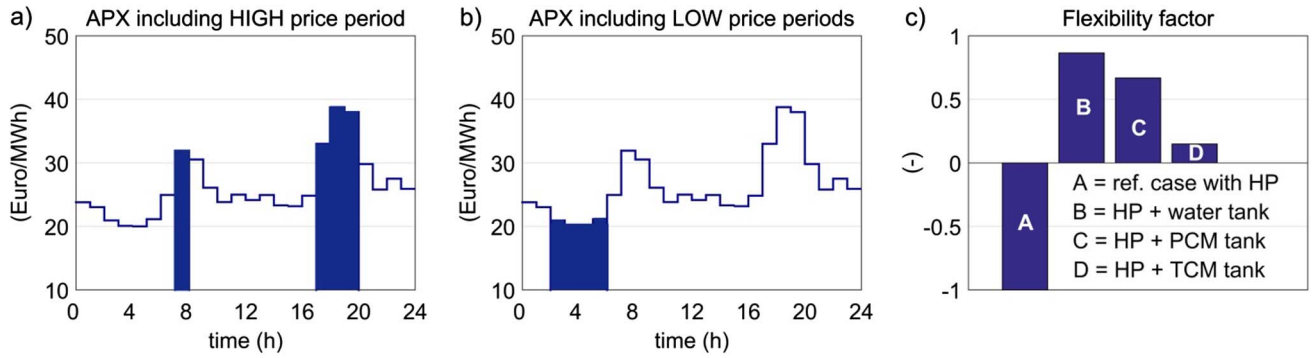

Fig. 14. Simulation results – flexibility related to operational electricity costs, hourly APX electricity prices including high price periods (a) and low price periods (b), (c) flexibility factor of different TES tanks in optimal control compared with reference control.

95 °C, the maximum temperature difference between PCM tank inlet and outlet is 10 K. Thus, only the electric heater is used to provide electrical instantaneous power flexibility which is similar to the thermal instantaneous power flexibility of 27–21 kW. At 12 am the PCM tank can be charged from 7% to 60% of energy capacity after about 60 min of flexibility time step regarding a charging temperature of 95 °C and a reference temperature of 21 °C. The change from 7% to 60% correlates to an energy uptake of 0.09 GJ. The instantaneous power flexibility of the TCM tank is the lowest among the TES tanks. For example at 12 am, charging with 95 °C results in a thermal power of 19 kW in the first 5 min of flexibility time step which is primarily due to the sensible heat stored in the TCM tank. From 5 to 60 min, thermal power decrease

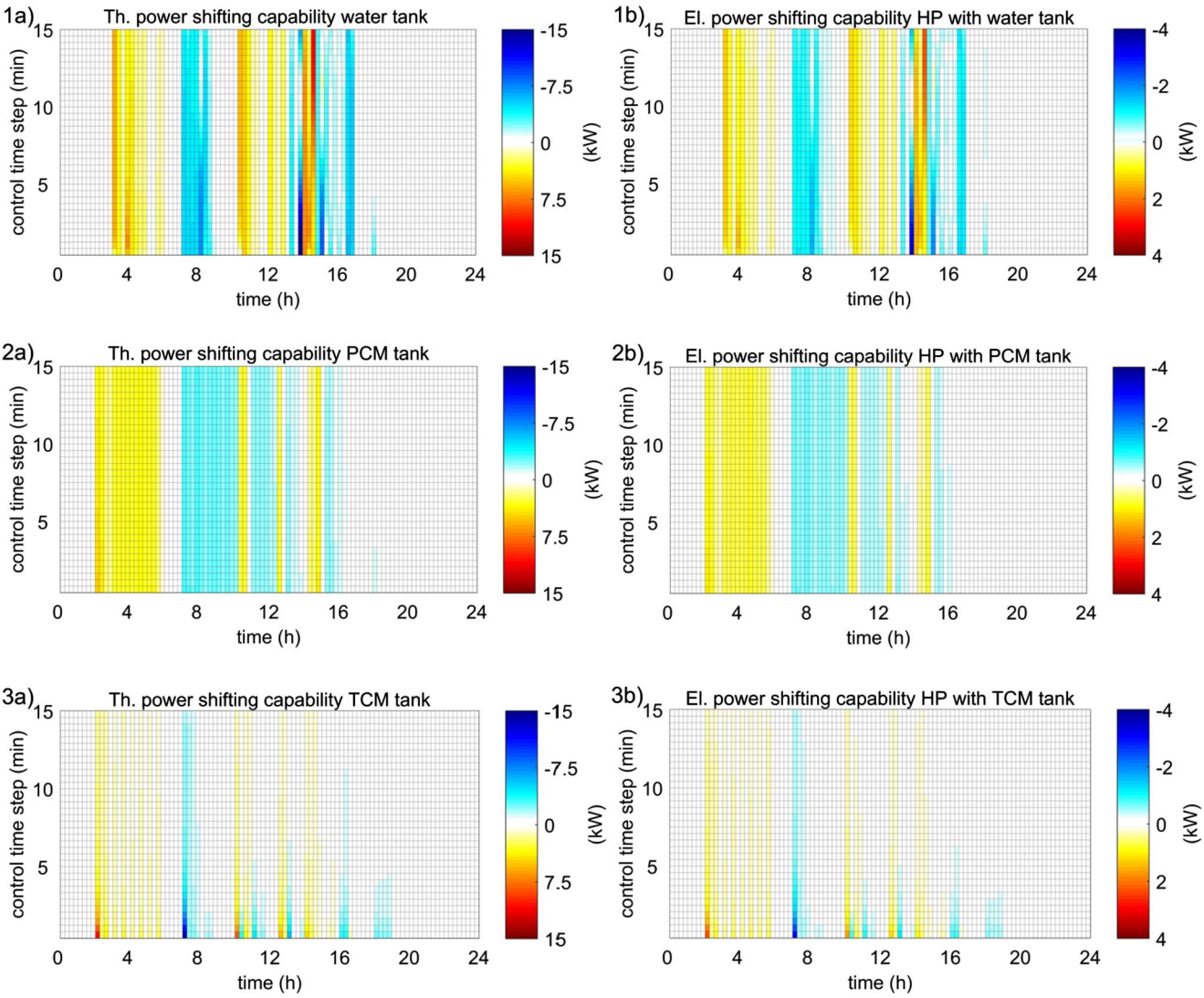

Fig. 15. Simulation results – power shifting capability comparing the power evolution between optimal and reference control for 1) water tank, 2) PCM tank, 3) TCM tank, a) thermal power shifting capability, b) electrical power shifting capability. The x-axis shows the control horizon of 24 h. The y-axis represents the 15 min control time step. During each control time step the evolving power flexibility is illustrated.

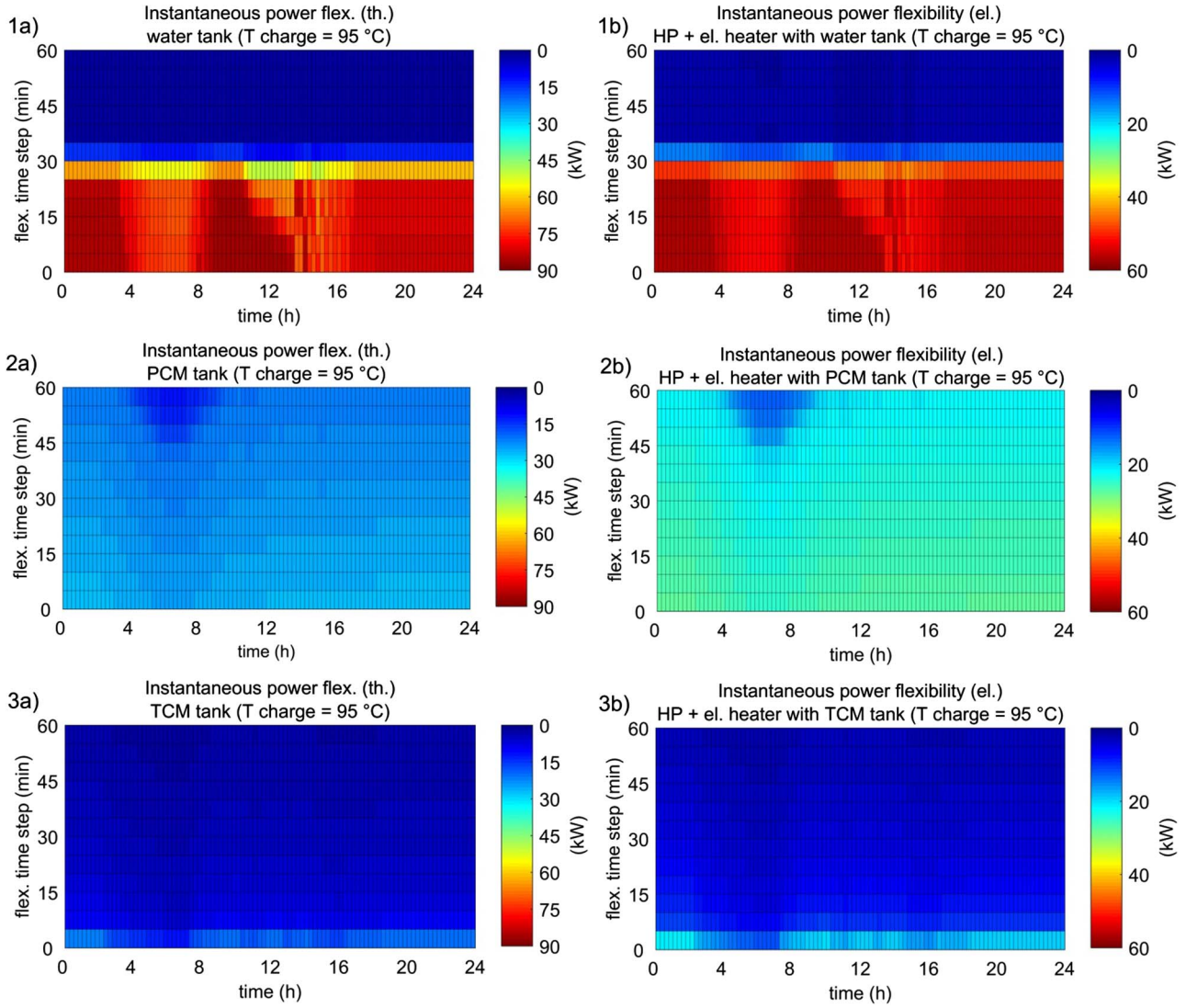

Fig. 16. Simulation results – instantaneous power flexibility for the charging case of TES with 95 °C based on the results of optimal control; 1) water tank, 2) PCM tank, 3) TCM tank; a) Inst. power flexibility (thermal), b) Inst. power flexibility (electrical). The x-axis shows the control horizon of 24 h. The y-axis represents the flexibility time step of 60 min in which the TES responds to a constant charging temperature of 95 °C. During the 60 min flexibility time step, the evolving power is illustrated at each control time step of the 24 h control horizon.

gradually from 10 to 3 kW that is due to the chemical energy stored in the TCM tank. The related energy capacity increases from 7% to 69% which is equal to an energy uptake of 0.03 GJ.

4. Discussion

Capturing heat and mass transfer dynamics is a prerequisite for determining demand flexibility of TES tanks integrated with building heating systems. To present this dynamic behavior with sufficient accuracy, TES models were developed based on a one-dimensional approach. The Crank-Nicolson scheme was applied to numerically solve conduction and diffusion for a one-dimensional configuration and reduce the computational effort for simulating TES tanks. The Crank Nicolson approach is a stable, robust, and powerful hybrid FD method. In combination with dynamic programming, Crank Nicolson was introduced and applied to simulate TES tanks in optimal control. The one-dimensional TES models consider simplifications regarding heat and mass transfer. For the packed-bed reactor using PCM, the one-dimensional problem solves the heat and mass transfer through the PCM layer in so far as the enthalpy distribution in the PCM layer is equal for the entire length of the heat exchanger. The PCM model does not include natural convection during the melting process, to facilitate the implementation into the optimization scheme and to reduce computational time. However, recent studies on PCM tanks have shown that natural convection can increase the heat transfer of the PCM in the solid-liquid interface [80–82]. For the packed-bed reactor using TCM, the one-dimensional problem solves the heat and mass transfer through the TCM layer. This simplification includes that the temperature and adsorbate distribution in the TCM layer are equal for the length of the heat exchanger. The one-dimensional approach for the water tank simulates the stratification of temperature segments. However, convection and conduction perpendicular to the height of the water tank are not included. Because previous studies have already successfully used the one-dimensional representation of water tanks [54–56], PCM tanks [57,58], and TCM tanks, for example in [59,60], the dynamic behavior of the TES tanks is sufficiently represented. However, a validation of the TES tank models using experimental data is recommended.

Demand flexibility related to energy is quantified using the performance indicators, storage capacity and storage efficiency. The calculated storage efficiency of the different TES tanks with optimal control is between 96 and 98% achieving a high performance compared to other studies [18].

Demand flexibility related to costs is expressed using the flexibility factor as performance indicator. The flexibility factor is significantly

increased by integrating TES tanks with optimal control. A limitation of the flexibility factor as a single indicator is that the results exclude a comparison to different building heating systems in different climate conditions. To overcome this limitation, this study has considered multiple flexibility indicators referring to energy, power, and costs.

Demand flexibility related to power is quantified using the shifting capability as a performance indicator. This indicator describes the difference of power usage between optimal and reference control. Because TES tanks are not considered in the reference control, the power shifting capability is identical to the dynamic response of the TES tanks in optimal control. Because the power shifting capability does not comprehensively represent the potential power flexibility of TES and power-to-heat, this paper has introduced the instantaneous power flexibility as performance indicator which shows the potential power flexibility of TES and power-to-heat in any case of charging, discharging or idle mode. The instantaneous power flexibility is calculated for a time scale of 1 h to determine grid ancillary services of short duration. The results for the power flexibility of TES are obtained with sufficient accuracy because detailed TES models are implemented to capture the complex storage dynamics. It becomes clear that more advanced TES tanks models are required in optimal control because simplified models cannot predict transition periods in which for example stratification in a water tank is not yet established and temperature distribution changes due to increased mixing of water.

In order to determine demand flexibility with TES tanks and power-to-heat, information of flexibility regarding energy, power, and costs have to be considered. It is observed that the water tank and PCM tank achieve highest energy flexibility compared to reference control. All TES tank show different behavior in the power flexibility. Water tanks can be charged quickly with high charging power and PCM tanks can be constantly charged for a longer time period with adequate charging power. The charging power may be regulated by changing the mass flow of the heat transfer medium that exchanges heat with the TES tank. A variable mass flow may enable more constant charging and discharging, but also introduces an additional operational parameter for optimization which results in an increase of the computational time for cost-optimal control.

5. Conclusion

In this study, the demand flexibility of TES tanks integrated with building heating system was determined showing that power-to-heat devices and water tanks, PCM tanks, and TCM tanks can be designed to provide flexibility of short duration (up to 24 h). To investigate the maximum building flexibility towards the power grid, optimal control of TES tanks, HP and electric heater was chosen. Optimal control considers the complexity of the building heating system and enables the integration of weather forecasting and prediction of internal gains. Because current grid signals commonly contain electricity prices, optimal control aims to minimizing the total operational electricity costs. When applying the developed optimal control framework to building energy management systems, real-time signals such as intra-day electricity prices can be implemented. The results of cost-optimal control showed that the water tank and the PCM tank achieve highest cost savings when comparing to reference control. However, no lifetime costs, lifecycle costs, or maintenance costs of the building heating system were assumed. The results of the cost-optimal control also show that the efficient use of electrical energy (COP of the heat pump) is similar to the reference control case. The simulated 24 h are only characteristically for an average day in the spring period and in the Netherlands. As next, different periods of the year and different climate conditions have to be simulated to gain a deeper insight into the system performance. However, this study aimed to determine demand flexibility of TES tanks integrated with building heating system. The demand flexibility is quantified using different performance indicators that sufficiently characterize flexibility in terms of size (energy), time (power) and costs. Energy flexibility with optimal control is expressed using the available storage capacity and storage efficiency indicating that all TES technologies, water tank, PCM tank, TCM tank and power-to-heat can enable energy flexibility towards the power grid. Flexibility related to costs is represented using the flexibility factor that sufficiently determines whether electricity is consumed during low or high electricity price periods. Power flexibility characterizes the evolution of heating power over time. The electrical power flexibility is directly linked to the power grid whereas the thermal flexibility shows the dynamic response of the heating system. The thermal and electrical power shifting capability was calculated to compare optimal control with reference control. However, the power shifting capability cannot be used to quantify the potential power flexibility of TES and power-to-heat in any case of charging, discharging or idle mode. Therefore, this paper has introduced the instantaneous power flexibility. Based on the results of the optimal control the instantaneous power flexibility is quantified for the charging case of 95 °C and a flexibility time step of 60 min.

The identification and quantification of demand flexibility is a crucial step towards electricity markets that can enable flexible energy consumption. Multiple flexibility indicators that relate to all dimensions of demand flexibility in terms of size (energy), time (power) and costs, will serve to determine demand flexibility. Therefore, it is required to use those flexibility indicators as a measure of the performance of control strategies in addition to conventional performance indicators such as energy consumption, costs, and energy efficiency.

In order to approach the optimization of multiple flexibility indicators in optimal control, future control strategies will implement flexibility indicators in the objective function. As an example, during periods of renewable power fluctuation, a building energy system, including TES, can be requested to increase or decrease power consumption to optimize load following and thus optimize the scheduling of TES and power-to-heat for power flexibility. In order to do that, a flexibility market mechanism must be established that allows to optimize for building demand flexibility.

Acknowledgement

This work is supported by BAM Techniek Energy Systems bv and BAM Bouw en Techniek Innovatie. This work is also included in the research activities of EBC Annex 67 Energy Flexible Buildings.

References

[1] Gelazanskas L, Gamage KAA. Demand side management in smart grid: A review and proposals for future direction. Sustain Cities Soc 2014;11:22–30. http://dx.doi.org/10.1016/j.scs.2013.11.001.
[2] Ottesen SO, Tomasgard A. A stochastic model for scheduling energy flexibility in buildings. Energy 2015;88:364–76. http://dx.doi.org/10.1016/j.energy.2015.05.049.
[3] Lopes RA, Chambel A, Neves J, Aelenei D, Martins J. A literature review of methodologies used to assess the energy flexibility of buildings. Energy Procedia 2016;91:1053–8. http://dx.doi.org/10.1016/j.egypro.2016.06.274.
[4] De Coninck R, Helsen L. Quantification of flexibility in buildings by cost curves – Methodology and application. Appl Energy 2016;162:653–65. http://dx.doi.org/10.1016/j.apenergy.2015.10.114.
[5] Kondziella H, Bruckner T. Flexibility requirements of renewable energy based electricity systems – a review of research results and methodologies. Renew Sustain Energy Rev 2016;53:10–22. http://dx.doi.org/10.1016/j.rser.2015.07.199.
[6] Stinner S, Huchtemann K, Müller D. Quantifying the operational flexibility of building energy systems with thermal energy storages. Appl Energy 2016;181:140–54. http://dx.doi.org/10.1016/j.apenergy.2016.08.055.
[7] Nuytten T, Claessens B, Paredis K, Van Bael J, Six D. Flexibility of a combined heat and power system with thermal energy storage for district heating. Appl Energy 2013;104:583–91. http://dx.doi.org/10.1016/j.apenergy.2012.11.029.
[8] D'hulst R, Labeeuw W, Beusen B, Claessens S, Deconinck G, Vanthournout K. Demand response flexibility and flexibility potential of residential smart appliances: Experiences from large pilot test in Belgium. Appl Energy 2015; 155: 79–90. doi:10.1016/j.apenergy.2015.05.101.
[9] Reynders G. Quantifying the impact of building design on the potential of structural storage for active demand response in residential. Buildings 2015.
[10] Le Dréau J, Heiselberg P. Energy flexibility of residential buildings using short term

heat storage in the thermal mass. Energy 2016;111:991–1002. http://dx.doi.org/10.1016/j.energy.2016.05.076.
[11] Clauß J, Finck C, Vogler-Finck P, Beagon P. Control strategies for building energy systems to unlock demand side flexibility – A review. Accepted paper at building simulation conference; 2017.
[12] Lund PD, Lindgren J, Mikkola J, Salpakari J. Review of energy system flexibility measures to enable high levels of variable renewable electricity. Renew Sustain Energy Rev 2015;45:785–807. http://dx.doi.org/10.1016/j.rser.2015.01.057.
[13] Oldewurtel F, Sturzenegger D, Andersson G, Morari M, Smith RS. Towards a standardized building assessment for demand response. IEEE 2013:7083–8. http://dx.doi.org/10.1109/CDC.2013.6761012.
[14] Salpakari J, Mikkola J, Lund PD. Improved flexibility with large-scale variable renewable power in cities through optimal demand side management and power-to-heat conversion. Energy Convers Manage 2016;126:649–61. http://dx.doi.org/10.1016/j.enconman.2016.08.041.
[15] Vanhoudt D, Geysen D, Claessens B, Leemans F, Jespers L, Van Bael J. An actively controlled residential heat pump: Potential on peak shaving and maximization of self-consumption of renewable energy. Renew Energy 2014;63:531–43. http://dx.doi.org/10.1016/j.renene.2013.10.021.
[16] Fischer D, Wolf T, Wapler J, Hollinger R, Madani H. Model-based flexibility assessment of a residential heat pump pool. Energy n.d. doi:10.1016/j.energy.2016.10.111.
[17] Fischer D, Madani H. On heat pumps in smart grids: A review. Renew Sustain Energy Rev 2017;70:342–57. http://dx.doi.org/10.1016/j.rser.2016.11.182.
[18] Reynders G, Diriken J, Saelens D. Generic characterization method for energy flexibility: Applied to structural thermal storage in residential buildings. Appl Energy 2017;198:192–202. http://dx.doi.org/10.1016/j.apenergy.2017.04.061.
[19] Salpakari J, Rasku T, Lindgren J, Lund PD. Flexibility of electric vehicles and space heating in net zero energy houses: an optimal control model with thermal dynamics and battery degradation. Appl Energy 2017;190:800–12. http://dx.doi.org/10.1016/j.apenergy.2017.01.005.
[20] Kim YJ, Fuentes E, Norford LK. Experimental study of grid frequency regulation ancillary service of a variable speed heat pump. IEEE Trans Power Syst 2016;31:3090–9. http://dx.doi.org/10.1109/TPWRS.2015.2472497.
[21] Fischer D, Lindberg KB, Madani H, Wittwer C. Impact of PV and variable prices on optimal system sizing for heat pumps and thermal storage. Energy Build 2016;128:723–33. http://dx.doi.org/10.1016/j.enbuild.2016.07.008.
[22] Arteconi A, Hewitt NJ, Polonara F. State of the art of thermal storage for demand-side management. Appl Energy 2012;93:371–89. http://dx.doi.org/10.1016/j.apenergy.2011.12.045.
[23] Navarro L, de Gracia A, Colclough S, Browne M, McCormack SJ, Griffiths P, et al. Thermal energy storage in building integrated thermal systems: A review. Part 1. Active storage systems. Renew Energy 2016;88:526–47. http://dx.doi.org/10.1016/j.renene.2015.11.040.
[24] Navarro L, de Gracia A, Niall D, Castell A, Browne M, McCormack SJ, et al. Thermal energy storage in building integrated thermal systems: A review. Part 2. Integration as passive system. Renew Energy 2016;85:1334–56. http://dx.doi.org/10.1016/j.renene.2015.06.064.
[25] Sterner M, Stadler I. Energiespeicher - Bedarf, Technologien, Integration. Berlin, Heidelberg: Springer, Berlin Heidelberg; 2014.
[26] Cabeza LF, Castell A, Barreneche C, de Gracia A, Fernández AI. Materials used as PCM in thermal energy storage in buildings: A review. Renew Sustain Energy Rev 2011;15:1675–95. http://dx.doi.org/10.1016/j.rser.2010.11.018.
[27] Cot-Gores J, Castell A, Cabeza LF. Thermochemical energy storage and conversion: A-state-of-the-art review of the experimental research under practical conditions. Renew Sustain Energy Rev 2012;16:5207–24. http://dx.doi.org/10.1016/j.rser.2012.04.007.
[28] Aydin D, Casey SP, Riffat S. The latest advancements on thermochemical heat storage systems. Renew Sustain Energy Rev 2015;41:356–67. http://dx.doi.org/10.1016/j.rser.2014.08.054.
[29] Finck C, Henquet E, van Soest C, Oversloot H, de Jong A-J, Cuypers R, et al. Experimental results of a 3 kWh thermochemical heat storage module for space heating application. Energy Procedia 2014;48:320–6. http://dx.doi.org/10.1016/j.egypro.2014.02.037.
[30] Zondag H, Kikkert B, Smeding S, de Boer R, Bakker M. Prototype thermochemical heat storage with open reactor system. Appl Energy 2013;109:360–5. http://dx.doi.org/10.1016/j.apenergy.2013.01.082.
[31] de Jong A-J, van Vliet L, Hoegaerts C, Roelands M, Cuypers R. Thermochemical heat storage – from reaction storage density to system storage density. Energy Procedia 2016;91:128–37. http://dx.doi.org/10.1016/j.egypro.2016.06.187.
[32] Mette B, Kerskes H, Drück H, Müller-Steinhagen H. New highly efficient regeneration process for thermochemical energy storage. Appl Energy 2013;109:352–9. http://dx.doi.org/10.1016/j.apenergy.2013.01.087.
[33] Masy G, Georges E, Verhelst C, Lemort V, André P. Smart grid energy flexible buildings through the use of heat pumps and building thermal mass as energy storage in the Belgian context. Sci Technol Built Environ 2015;21:800–11. http://dx.doi.org/10.1080/23744731.2015.1035590.
[34] Arteconi A, Hewitt NJ, Polonara F. Domestic demand-side management (DSM): Role of heat pumps and thermal energy storage (TES) systems. Appl Therm Eng 2013;51:155–65. http://dx.doi.org/10.1016/j.applthermaleng.2012.09.023.
[35] Patteeuw D, Bruninx K, Arteconi A, Delarue E. D'haeseleer W, Helsen L. Integrated modeling of active demand response with electric heating systems coupled to thermal energy storage systems. Appl Energy 2015;151:306–19. http://dx.doi.org/10.1016/j.apenergy.2015.04.014.
[36] Mikkola J, Lund PD. Modeling flexibility and optimal use of existing power plants with large-scale variable renewable power schemes. Energy 2016;112:364–75. http://dx.doi.org/10.1016/j.energy.2016.06.082.
[37] Berkenkamp F, Gwerder M. Hybrid model predictive control of stratified thermal storages in buildings. Energy Build 2014;84:233–40. http://dx.doi.org/10.1016/j.enbuild.2014.07.052.
[38] Schütz T, Streblow R, Müller D. A comparison of thermal energy storage models for building energy system optimization. Energy Build 2015;93:23–31. http://dx.doi.org/10.1016/j.enbuild.2015.02.031.
[39] Salpakari J, Lund P. Optimal and rule-based control strategies for energy flexibility in buildings with PV. Appl Energy 2016;161:425–36. http://dx.doi.org/10.1016/j.apenergy.2015.10.036.
[40] Renaldi R, Kiprakis A, Friedrich D. An optimisation framework for thermal energy storage integration in a residential heat pump heating system. Appl Energy n.d. doi:10.1016/j.apenergy.2016.02.067.
[41] Gambino G, Verrilli F, Canelli M, Russo A, Himanka M, Sasso M, et al. Optimal operation of a district heating power plant with thermal energy storage. IEEE 2016:2334–9. http://dx.doi.org/10.1109/ACC.2016.7525266.
[42] Finck C. An optimization strategy for scheduling various thermal energy storage technologies in office buildings connected to smart grid. Energy Procedia 2015.
[43] Touretzky CR, Salliot AA, Lefevre L, Baldea M. Optimal operation of phase-change thermal energy storage for a commercial building. IEEE 2015:980–5. http://dx.doi.org/10.1109/ACC.2015.7170861.
[44] Fiorentini M, Cooper P, Ma Z, Robinson DA. Hybrid model predictive control of a residential HVAC system with PVT energy generation and PCM thermal storage. Energy Procedia 2015;83:21–30. http://dx.doi.org/10.1016/j.egypro.2015.12.192.
[45] Verrilli F, Srinivasan S, Gambino G, Canelli M, Himanka M, Del Vecchio C, et al. Model predictive control-based optimal operations of district heating system with thermal energy storage and flexible loads. IEEE Trans Autom Sci Eng 2016:1–11. http://dx.doi.org/10.1109/TASE.2016.2618948.
[46] Touretzky CR, Baldea M. A hierarchical scheduling and control strategy for thermal energy storage systems. Energy Build 2016;110:94–107. http://dx.doi.org/10.1016/j.enbuild.2015.09.049.
[47] Fazlollahi S, Becker G, Maréchal F. Multi-objectives, multi-period optimization of district energy systems: II—Daily thermal storage. Comput Chem Eng n.d. doi:10.1016/j.compchemeng.2013.10.016.
[48] Alimohammadisagvand B, Jokisalo J, Kilpeläinen S, Ali M, Sirén K. Cost-optimal thermal energy storage system for a residential building with heat pump heating and demand response control. Appl Energy 2016;174:275–87. http://dx.doi.org/10.1016/j.apenergy.2016.04.013.
[49] Dimplex Technische Daten Luft/Wasser Wärmepumpe LA 18S-TU n.d. http://www.dimplex.de/pdf/de/produktattribute/produkt_1727910_extern_egd.pdf [accessed September 23, 2016].
[50] Finck C, Li R, Zeiler W. Operational load shaping of office buildings connected to thermal energy storage using dynamic programming. In: Proc. 12th REHVA world congr. vol. 10 Pap. 70, Aalborg: Aalborg University; 2016.
[51] Sturzenegger D, Gyalistras D, Semeraro V, Morari M, Smith RS. BRCM Matlab toolbox: Model generation for model predictive building control. In: Am. control conf. ACC 2014, IEEE; 2014. p. 1063–9.
[52] Recknagel H, Sprenger E, Schramek E-R. Taschenbuch für Heizung + Klimatechnik 07/08: Taschenbuch für Heizung + Klimatechnik 2007/2008. einschließlich Warmwasser- und Kältetechnik. 73rd ed. München u.a.: Deutscher Industrieverlag; 2006.
[53] Armacell_Produktkatalog_2016_DE_low.pdf n.d. http://www.armacell.com/WWW/armacell/ACwwwAttach.nsf/ansFiles/Armacell_Produktkatalog_2016_DE_low.pdf/$File/Armacell_Produktkatalog_2016_DE_low.pdf [accessed August 23, 2016].
[54] Shukla A, Singh AK, Singh P, Shukla A, Singh AK, Singh P. A comparative study of finite volume method and finite difference method for convection-diffusion problem. Am J Comput Appl Math 2011;1:67–73.
[55] Appadu AR. Numerical solution of the 1D advection-diffusion equation using standard and nonstandard finite difference schemes. J Appl Math 2013. http://dx.doi.org/10.1155/2013/734374.
[56] Karahan H. Implicit finite difference techniques for the advection–diffusion equation using spreadsheets. Adv Eng Softw 2006;37:601–8. http://dx.doi.org/10.1016/j.advengsoft.2006.01.003.
[57] Lo Brano V, Ciulla G, Piacentino A, Cardona F. Finite difference thermal model of a latent heat storage system coupled with a photovoltaic device: Description and experimental validation. Renew Energy 2014;68:181–93. http://dx.doi.org/10.1016/j.renene.2014.01.043.
[58] Hu H, Argyropoulos SA. Mathematical modelling of solidification and melting: a review. Model Simul Mater Sci Eng 1996;4:371. http://dx.doi.org/10.1088/0965-0393/4/4/004.
[59] Pesaran A, Lee H, Hwang Y, Radermacher R, Chun H-H. Review article: Numerical simulation of adsorption heat pumps. Energy 2016;100:310–20. http://dx.doi.org/10.1016/j.energy.2016.01.103.
[60] Finck CJ, Spijker JC van 't, Jong AJ de, Henquet EMR, Oversloot HP, Cuypers R. Design of a modular 3 kWh thermochemical heat storage system for space heating application n.d.
[61] Morton KW. Numerical solution of convection-diffusion problems. London: Chapman & Hall; 1996.
[62] Kanzow C. Numerik Linearer Gleichungssysteme: Direkte und iterative Verfahren. 2005th ed. Berlin: Springer; 2005.
[63] Wiley: Numerical computation of internal and external flows, Volume 1: fundamentals of numerical discretization - Charles Hirsch n.d. http://www.wiley.com/WileyCDA/WileyTitle/productCd-0471923850.html [accessed June 7, 2017].
[64] Cooper JM. Introduction to partial differential equations with MATLAB. Corrected edition Boston: Birkhäuser; 2000.
[65] Recktenwald GW. Numerical methods with MATLAB: implementations and

applications. Prentice Hall; 2000.
[66] Trefethen numerical ODE/PDE textbook n.d. http://people.maths.ox.ac.uk/trefethen/pdetext.html [accessed July 25, 2016].
[67] Kenisarin MM. Thermophysical properties of some organic phase change materials for latent heat storage. A review. Sol Energy 2014;107:553–75. http://dx.doi.org/10.1016/j.solener.2014.05.001.
[68] Kenisarin M, Mahkamov K. Salt hydrates as latent heat storage materials: Thermophysical properties and costs. Sol Energy Mater Sol Cells 2016; 145, Part 3: 255–86. doi:10.1016/j.solmat.2015.10.029.
[69] Mosaffa AH, Garousi Farshi L, Infante Ferreira CA, Rosen MA. Energy and exergy evaluation of a multiple-PCM thermal storage unit for free cooling applications. Renew Energy 2014;68:452–8. http://dx.doi.org/10.1016/j.renene.2014.02.025.
[70] Levin PP, Shitzer A, Hetsroni G. Numerical optimization of a PCM-based heat sink with internal fins. Int J Heat Mass Transf 2013;61:638–45. http://dx.doi.org/10.1016/j.ijheatmasstransfer.2013.01.056.
[71] de Jong A-J, Trausel F, Finck C, van Vliet L, Cuypers R. Thermochemical heat storage – system design issues. Energy Procedia 2014;48:309–19. http://dx.doi.org/10.1016/j.egypro.2014.02.036.
[72] Trausel F, de Jong A-J, Cuypers R. A review on the properties of salt hydrates for thermochemical storage. Energy Procedia 2014;48:447–52. http://dx.doi.org/10.1016/j.egypro.2014.02.053.
[73] Rindt CCM, Gaastra-Nedea SV. 15 - Modeling thermochemical reactions in thermal energy storage systems. In: Cabeza LF, editor. Adv. Therm. Energy Storage Syst., Woodhead Publishing; 2015. p. 375–415.
[74] Wang Y, LeVan MD. Adsorption equilibrium of carbon dioxide and water vapor on zeolites 5A and 13X and silica gel: pure components. ResearchGate 2009; 54. doi:10.1021/je800900a.
[75] Sayılgan ŞÇ, Mobedi M, Ülkü S. Effect of regeneration temperature on adsorption equilibria and mass diffusivity of zeolite 13x-water pair. Microporous Mesoporous Mater 2016;224:9–16. http://dx.doi.org/10.1016/j.micromeso.2015.10.041.
[76] Leong KC, Liu Y. System performance of a combined heat and mass recovery adsorption cooling cycle: A parametric study. Int J Heat Mass Transf 2006;49:2703–11. http://dx.doi.org/10.1016/j.ijheatmasstransfer.2006.01.012.
[77] Dobbs JR, Hencey BM. Predictive HVAC control using a Markov occupancy model. Am. Control Conf. ACC 2014;2014:1057–62. http://dx.doi.org/10.1109/ACC.2014.6859389.
[78] Bertsekas DP. Dynamic programming and optimal control. Belmont, Mass.: Athena Scientific; 2005.
[79] Finck C, Li R, Zeiler W. Performance maps for the control of thermal energy storage. Accepted paper at building simulation conference 2017.
[80] Padovan R, Manzan M. Genetic optimization of a PCM enhanced storage tank for solar domestic hot water systems. Sol Energy 2014;103:563–73. http://dx.doi.org/10.1016/j.solener.2013.12.034.
[81] Izquierdo-Barrientos MA, Sobrino C, Almendros-Ibáñez JA. Modeling and experiments of energy storage in a packed bed with PCM. Int J Multiph Flow 2016;86:1–9. http://dx.doi.org/10.1016/j.ijmultiphaseflow.2016.02.004.
[82] Jmal I, Baccar M. Numerical study of PCM solidification in a finned tube thermal storage including natural convection. Appl Therm Eng 2015;84:320–30. http://dx.doi.org/10.1016/j.applthermaleng.2015.03.065.